University College of Southeast Norway

www.usn.no

FMH606 Master's Thesis 2017

System and Control Engineering

Heat transfer mechanisms in MV load break switches

Stein Øygarden

Faculty of Technology, Natural Sciences and Maritime Sciences

Campus Porsgrunn

University College of Southeast Norway

www.usn.no

Course: FMH606 Master's Thesis, 2017

Title: Heat transfer mechanisms in MV load break switches

Number of pages: 59

Keywords: MV Switchgear, Knife switch, Puffer switch, Temperature measurements, Heat transfer, Effects of encapsulation,

Student: Stein Øygarden

Supervisor: Elin Fjeld and Wilhelm Rondeel

External partner: ABB AS

Availability: Open

Approved for archiving: _____
(supervisor signature)

Summary:

This report is part of an ongoing research project between University college of Southeast Norway and ABB Power product division. This report focuses on the heat transfer from two load break switch (LBS), normally used in gas-insulated switchgears. The two LBS designs examined are the knife and puffer switch. How the heat transfer from the conductive paths, in both LBS designs, are affected by the encapsulating structures are investigated.

There have been conducted temperature measurements with and without the structures, inside air-filled enclosures. Calculations of the heat transfer from both LBS designs and theoretical calculations of encapsulation have been conducted.

For both LBS designs the structures have small effects on the temperatures rise. For the knife switch, there were small changes in distribution of the heat transfer mechanisms. For the puffer switch the effect of radiation increases, when the structures are added, from 7 % to 50 % of the total power loss. The convection decreases, when the structures are added to the LBS, from 76 % to 35 % for the puffer switch. The reason for changes in distribution of heat transfer mechanisms for the puffer switch, is a higher percentage of encapsulation (with higher emissivity coefficient) and changed surface area. The power loss due to conduction was approximately 15 % for both LBS designs with and without encapsulation.

Preface

This report is a result of the master's thesis "Heat transfer mechanisms in MV load break switches". This report is a part of an ongoing research project between University College of Southeast Norway (USN) and ABB Power Products Division, in Skien, Norway.

This report is written during the final semester of the master degree in System and Control Engineering at USN.

I would like to thank the supervisors Elin Fjeld and Wilhelm Rondeel for their time and valuable help during this period.

Porsgrunn, 15.05.2017

Stein Øygarden

Nomenclature

AC – Alternating current

DC – Direct current

LBS – Load break switch

IEC – International Electrotechnical Commission

Cu – Copper

USN – University College of Southeast Norway

Ni – Nickel

Cr – Chromium

Steady state – temperature increase less than 1 °C per hour[1].

Symbols used in this report:

P – Power (W)

R – Resistance (Ω)

I – Current (A)

ρ – Electrical resistivity (Ω*m)

L – Length (m)

A – Cross section (m^2)

α – Temperature coefficient (1/K)

Δ – Delta (Change in)

c – Specific heat (J/(kg*K))

γ – Density (kg/m^3)

h – Heat transfer coefficient (W/m^2*K)

V – Volume (m^3)

λ – Thermal conductivity (W/m*K)

σ_s – Stefan Boltzmann's constant

U – Surface area (m^2)

T – Surface temperature (ºK)

f – Factor to compensate for the surroundings

g – gravity (m/s^2)

β – Thermal expansion coefficient (1/K)

η – Kinematic viscosity (m^2/s)

μ – Dynamic viscosity (kg/m*s)

ε – Emissivity

D – Diameter (m)

r – Radius (m)

$\dot{Q}$ – Heat flow (W)

c – Specific heat (J/(kg*K))

Contents

Preface 3

Nomenclature 4

Contents 5

1 Introduction 7

1.1 Background 7
1.2 Objectives 8
1.3 Report structure 8

2 Theory 10

2.1 Switchgear 10
2.1.1 Knife switch *10*
2.1.2 Puffer switch *10*
2.2 Heat Generation 11
2.3 Heat transfer 13
2.3.1 Conduction *14*
2.3.2 Radiation *15*
2.3.3 Convection *15*
2.4 Total heat transfer coefficient 17

3 Method 19

3.1 System description 19
3.1.1 Switchgear with knife switch *19*
3.1.2 Switchgear with puffer switch *21*
3.2 Equipment used 24
3.2.1 Thermocouple *25*
3.3 Finding the emissivity coefficient for a material 25
3.4 Resistance measurement 26
3.5 Temperature measurements 26
3.5.1 For estimating the contribution of conduction *26*
3.5.2 For estimating the contribution of convection *27*
3.5.3 For estimating the contribution of radiation *29*

4 Results 31

4.1 Power input 31
4.2 Temperature measurements 31
4.3 Heat transfer calculations 35

5 Theoretical calculations of encapsulation 38

5.1 Introduction to encapsulation of conductors 38
5.1.1 Thermal conductivity of air cavities *38*
5.2 Simplified model of LBS 39
5.3 Theory of encapsulation of a cylindrical conductor 40
5.4 Results of theoretical calculations of encapsulation 40

6 Discussion 42

6.1 Emissivity measurement 42
6.2 Knife switch 42
6.3 Puffer switch 43

6.4 Theoretical convective heat transfer coefficient 45

7 .. Conclusion 46

References 47

Appendices 49

1 Introduction

In this chapter, an introduction to the background and the system examined in this report will be given. Then the objectives of this report will be presented. In the end of this chapter, the structure of this report is presented.

1.1 Background

In the power grid, it is necessary to be able to disconnect the power. To disconnect the power a switchgear, also referred to as ring unit, can be used. Switchgears contains often a circuit breaker for breaking huge currents when faults occur in the power grid and load break switches (LBS) for making or breaking the connection during normal conditions. Figure 1-1 shows a normal arrangement of a power grid with switchgears. This setup makes it possible to keep the customers connected even when a fault has occurred. The area where the fault has occurred can be disconnected and repaired. To be able to do this the grid is connected in rings as shown in Figure 1-1.

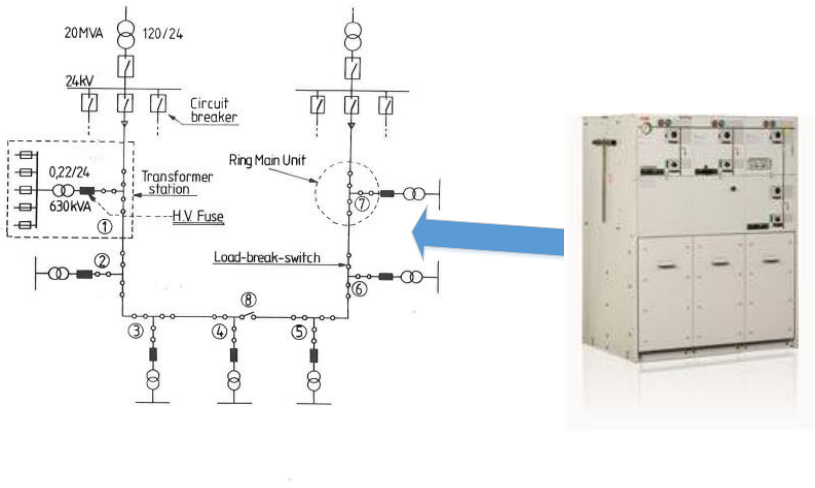

Figure 1-1: Sketch of a grid showing a typical position of a switchgear.[2, 3]

There are different ways of categorizing switchgears, for example by voltage levels. There are three different voltage levels often used to categorize the switchgears, these are: [4]

- Low voltage — less than 1 kV AC
- Medium voltage — 1 – 35 kV AC
- High voltage — more than 35 kV AC

Which type of isolation medium being used, is another method of categorizing the switchgears. Typical types of isolation mediums used in switchgears are SF_6, oil and vacuum [4]. Switchgears uses isolation mediums to be able to make the switchgears more compact. The isolation mediums improve the capability for arc quenching and gives better thermal properties. The most used isolation medium in switchgears is sulfur hexafluoride (SF_6). This is a very potent greenhouse gas, as much as 23 900 times worse than CO_2[5]. This is the main reason why the manufacturers of switchgears want to find a replacement for this gas. Air would be the preferred replacement of SF_6. Replacing SF_6 with air creates three main problems. One of them

is that SF_6 has better dielectric properties than air. The SF_6 gas is also better at quenching the arcs created when connecting and disconnecting the power. The last problem when air is replacing SF_6, is that the thermal properties of SF_6 are much better than air. ABB want to find a method to estimate the temperature rise in future designs, before making a prototype to physically measure the temperatures. The temperature limits of the different parts in a switchgear are set by the International Electrical Commission (IEC) and can be found in the international standard IEC 62271-1[6]. ABB in cooperation with USN have started a research project to create a method to predict the temperature rise in future designs. This master thesis will be a part of this ongoing research project. [7]

In this report, two different types of LBS designs will be examined, knife switch and puffer switch. Both switches are, to a different extent, encapsulated by plastic material. The encapsulation is necessary for the switches to work properly.

In this report, both LBS designs will be tested with and without the natural encapsulation. These tests are conducted to estimate how encapsulation affects the heat transfer of the LBS. The scope of this report will further be presented in chapter 1.2 Objectives.

1.2 Objectives

The objective from the task description in Appendix A is shown below:

"The proposed Master's thesis will be a part of the ongoing project between HSN and ABB. The student should calculate heat transfer coefficients for critical parts by considering the different heat transport mechanisms (convection, radiation and conduction). Temperature measurements should be performed with and without including the structures and the students should investigate how these structures affect the heat transport away from the hot spots."

The critical parts in this report are defined as the LBS [1]. Temperatures measurements shall be performed on the two different switchgear installations, which are provided by ABB and are available at USN. The switchgears contain two different types of LBS designs. Heat transfer calculations shall be performed for both switches. How the structures affect the heat transfer for both LBS designs shall be investigated.

1.3 Report structure

This report consists of 7 main chapters.

Chapter 1: Introduction

Gives a short introduction to the topics of this report

Chapter 2: Theory

The theory used in this report is presented

Chapter 3: Method

First, a system description is given before the equipment that has been used and the method for measuring the results is presented.

Chapter 4: Results

In this section the results of the report is displayed

Chapter 5 Theoretical calculations of encapsulation

This chapter is divided into three parts. In the first part an introduction theory used in this section will be given. Then a simplified model of the LBS is presented. In part number three the mathematic of this theory will be presented. In the last section, the results will be displayed.

Chapter 6: Discussion

In this section the results found in this report will be discussed

Chapter 7: Conclusion

In the last section of this report a conclusion of the discussion will be presented.

2 Theory

In this chapter the theory used in this report will be presented. First a short introduction to the two different LBS designs will be given. Then the heat generation in a system will be explained. In the end of this chapter the different heat transfer mechanisms will be explained and the theory used for estimating the heat transfer will be introduced.

2.1 Switchgear

In this report, two different types of MV switchgears will be examined. The main difference between these switchgears is the different types of LBS designs, knife switches and puffer switches. These two types of LBS will be presented in the next subchapters.

2.1.1 Knife switch

The first LBS to be examined is the knife switch, shown in Figure 2-1. The conductive parts in the knife switch are made of silver coated copper. In Figure 2-1, a sketch of a single knife switch is shown, with naming of essential parts. In this sketch a plastic piece is surrounding the knifes. Further in this report this plastic piece will be referred to as the insulating lever. The lever pulls the knife from open to closed position by a rod connected to the two holes shown in Figure 2-1. The insulating lever is made of Lexan 3413, which is a material made of polycarbonate with 30% fiberglass[8]. The structure to be investigated for the knife switch is the insulating lever. [1]

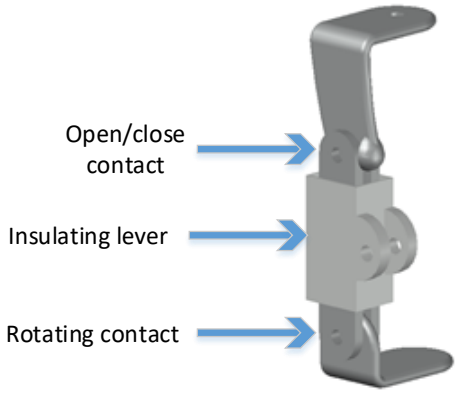

Figure 2-1: Knife switch with insulating lever.

2.1.2 Puffer switch

The puffer switch is operated by a rotating shaft, which operates the open/close contact.Figure 2-2, shows a sketch of the puffer switch, with naming of essential parts This switch is normally almost completely encapsulated. The encapsulation consists mostly of plastic, but the field controllers consist of aluminium. In Figure 2-2, the field controllers are removed. The field controllers are a cylindrical cap on top of the pressure cylinder and two rings mounted to a plate on the bottom of the Cu bar.

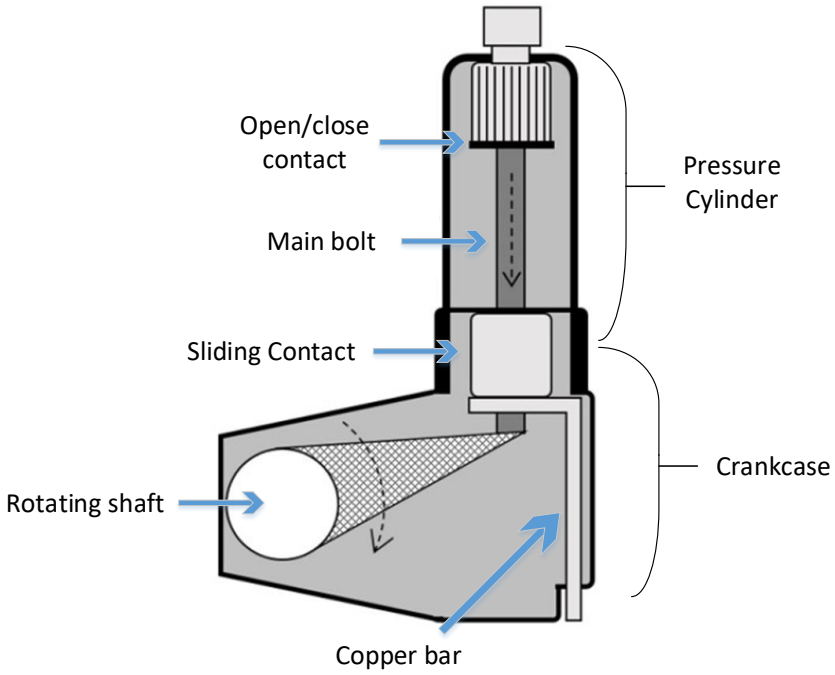

Figure 2-2: Puffer switch with and without encapsulation. (figure 2 in [1])

In Figure 2-2, the encapsulation is separated into two parts, the pressure cylinder and the crankcase. These two names will be used further in the report when the encapsulating parts are referred to. The plastic covers surrounding the LBS is essential for the puffer switch to work properly. The pressure cylinder makes the main bolt work as a piston blowing at the arc. The pressure cylinder is made of PA-63 Trogamid T5000 NL. The crankcase is converting the forces of the roaring shaft to a linear movement of the main bolt, which operates the Open/close contact. The crankcase is made of PBT- Tecodur PB 70 NL IL. The structures to be investigated for the puffer switch are the pressure cylinder and the crankcase [1]

2.2 Heat Generation

When current is flowing through the conductors in the switchgear the temperature will increase due to ohmic losses, equation (2.1).

$$P_{total} = R \cdot I^2 \tag{2.1}$$

P_{total} = Generated heat (W)

R = Resistance (Ω)

I = Current (A)

The total ohmic losses are the sum of the bulk resistance and the contact resistance, equation (2.2).

$$R = R_{bulk} + R_{contact} \tag{2.2}$$

R = Resistance (Ω)

The bulk resistance is the resistance in the material of the conductor. Bulk resistance is affected by the temperature. The bulk resistance can be found using equation (2.3).

$$R_{bulk} = \rho \cdot \frac{L}{A} \tag{2.3}$$

$\rho =$ Electrical resistivity (Ω*m)

$L =$ Length of conductor (m)

$A =$ Cross section of the conductor (m^2)

Equation (2.4), explains the relationship between the electrical resistivity and change in temperature.

$$\rho = \rho_0 \cdot (1 + \alpha \cdot \Delta T) \tag{2.4}$$

ρ_0 = Electrical resistivity at 20 ºC (Ω*m)

α = Temperature coefficient (1/°C)

ΔT = Change in temperature from 20 °C

The contact resistance is the resistance created between two conductors pressed together. The different contacts in the switchgears are bolted contacts, open/close contact, rotating contacts and sliding contacts. Contact resistance and the bulk resistance will generate heat in the switchgears. The amount of power loss due to ohmic resistance can be found by using equation (2.1) presented earlier.

When the LBS are connected to power, the temperature of the conductors will start to increase due to ohmic losses. Contribution from skin effect or iron losses are small and can be neglected [9]. Gradually as the temperature increases it will start to transfer heat to the surroundings. After some time, the temperature has reached a steady state temperature. Then all the heat generated will be transferred to the surroundings. Equation (2.5), should be introduced to explain the contribution between heat generated in the conductor and the heat transfer to the surrounding.

$$c \cdot \gamma \cdot V \cdot \frac{d}{dt} \cdot \Delta T + h \cdot U \cdot \Delta T = R \cdot I^2 \tag{2.5}$$

$c =$ Specific heat (J/(kg*K))

$\gamma =$ Density (kg/m^3)

$V =$ Volume of conductor (m^3)

$\Delta T =$ Temperature difference (K)

$h =$ Heat transfer coefficient (W/m^2*K)

$U =$ Surface area (m^2)

$L =$ Length of conductor (m)

The first term in the equation (2.5), is for calculating how much power used to heat up the conductor. In the moment power is connected, the heat transfer coefficient (h) and the change in temperature are too small to affect the power loss. Because of this, in the beginning most of

the power loss will contribute to heating up the conductor. The second term in equation (2.5) is for calculating how much power is transferred to the surroundings. When the power is turned on ΔT will be close to zero. When ΔT increases more of the power loss will be transferred to the surrounding. After a while, the power transferred to the surroundings will be equal to the total power loss. Because of this, the conductors will reach a maximum temperature. This temperature is called steady temperature. Steady state temperature is defined as when the increase is less than 1 ºC per hour[1]. Figure 2-3 shows the temperature rise of a conductor as a function of time. The arrows from the equation in Figure 2-3 is showing in which stage of the heating process the different terms is contributing to the highest power loss. [2]

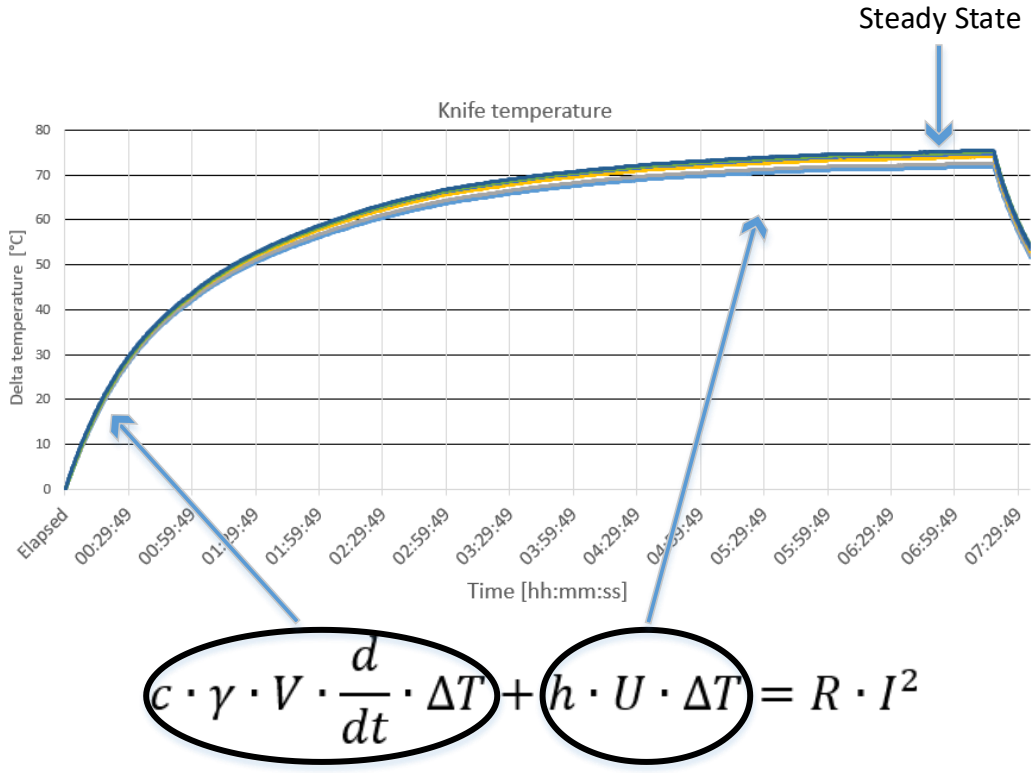

Figure 2-3: Temperature rise of a conductor as a function of time.(Inspired by 6.24 in [2])

This report, are looking at the steady state case of this process and the fundamental principles of heat transfer to the surroundings will be explained in chapter 2.3 Heat transfer.

2.3 Heat transfer

When heat is generated it will always travel towards colder areas. There are three different types of heat transfer and these are conduction, convection and radiation and will be explained in the following subchapters.

As stated earlier, when a steady state case is examined all the consumed power will contribute to heat transferred to the surroundings. Equation (2.1), in chapter 2.2 Heat Generation, can be used to calculate the total amount of power transferred to the surrounding.

Since the heat transfer to the surroundings only can happen through conduction, convection and radiation, P_{total} can be expressed as:

$$P_{total} = P_{conduction} + P_{convection} + P_{radiation} \quad (2.6)$$

In Figure 2-4, the three different heat transfer mechanisms are illustrated in a switchgear. In the next three subchapters conduction, convection and radiation will be explained.

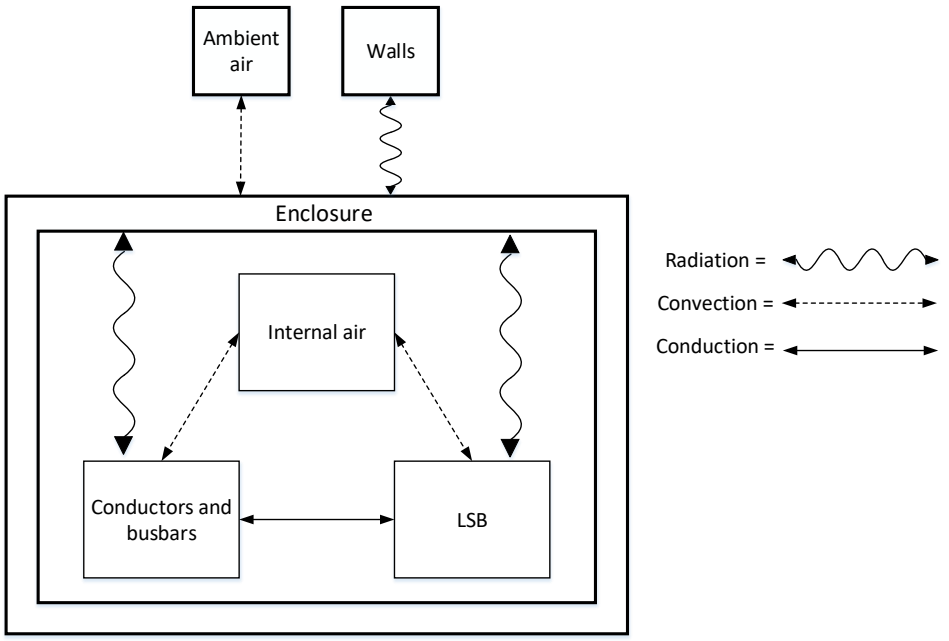

Figure 2-4: Explaining the three types of heat transfer in a switchgear. (Inspired by figure 6.6 in [2])

2.3.1 Conduction

Conduction is when the heat flows within a solid body. This means when heating up one end of a rod, the temperature will increase along the rod as well. The LBS, can transfer heat through conduction upward to the busbar or downwards to the outlet conductor, shown in Figure 2-4.

The conduction is effected by type of material. Some materials conduct heat better than others, for example silver is a good heat conductor. To find how much heat is transferred through conduction, the temperature difference and the dimensions must be known and this can be used in equation (2.7) to calculate the amount of power transferred. [2]

$$P_{conduction} = \frac{\lambda}{L} \cdot A \cdot \Delta T \quad (2.7)$$

$P_{conduction}$ = Heat flow (W)

λ = Thermal conductivity (W/ (m *K))

L = Distance between measuring points (m)

A = Cross section of conductor (m^2)

ΔT = Temperature difference along the distance L (ºC or K)

For using equation (2.7) to calculate the conduction an assumption is made. This assumption is that the power loss due to the bulk resistance and the heat transfer due to other effects is neglected between the measuring points.[1]

2.3.2 Radiation

Radiation is electromagnetic waves sent from a hot object. The heat transfer due to radiation in Figure 2-4 is between the hotter parts and the colder parts. The hotter parts are the conducting parts and the colder parts are the walls of the enclosure. To calculate the effect of radiation, equation (2.8) can be used. [2]

$$P_{radiation} = \varepsilon \cdot \sigma_s \cdot U \cdot (T_s^4 - T_0^4) \cdot f \quad (2.8)$$

$P_{radiation}$ = Heat flow (W)

ε = Emissivity

σ_s = Stefan Boltzmann's constant

U = Surface area (m^2)

T_s = Surface temperature (ºK)

T_0 = Wall temperature (ºK)

f = Factor to compensate for the surroundings

The factor f is to compensate for the surroundings. The switches are surrounded by other hot parts inside the enclosure. When two equally hot objects with the same emissivity are placed next to each other. These objects will transmit the same amount of radiation as they receive in the direction where they are facing each other. In Table 2-1, the factors for compensating for the surroundings used in this report can be found for both LBS designs. The factors presented in Table 2-1, are found in paper by Elin Fjeld et al. [1]

Table 2-1: Factors used for compensating for surroundings in the calculations. [1]

Type of Switch	Factor
Knife Switch	0,8
Puffer Switch	0,7

2.3.3 Convection

Convection is when a liquid or a gas is cooling an object by natural or forced contact with the solid body. Forced convection can be a fan blowing on a hot object. Natural convection is the movement in the liquid or gasses due to temperature differences and is also affected by the gravity. Convection from the LBS, in Figure 2-4, is transferring heat to the surrounding air inside the enclosure. The power loss due to convection can be calculated by using equation (2.9). [2]

$$P_{convection} = h_{conv} \cdot U \cdot (T_s - T_0) \quad (2.9)$$

$P_{convection}$ = Heat flow (W)

h_{conv} = Convective heat transfer coefficient (W/m^2*K)

U = Surface area (m^2)

T_s = Temperature of hot surface (K)

T_0 = Temperature of surrounding air (K)

When using equation (2.9) to calculate the power loss due to convection, the convective heat transfer coefficient must be known. The convective heat transfer coefficient can be found either by an empirical method or a theoretical method. To find the empirical convective heat transfer coefficient, the radiation and the conduction are calculated. Then the total power loss is used to find power loss due to convection, equation (2.10).

$$P_{conv} = P_{total} - P_{cond} - P_{rad} \tag{2.10}$$

When power loss due to convection have been found, equation (2.9) can be used to find the convective heat transfer coefficient.

Another possibility is to calculate the heat transfer coefficient theoretically. The method used for finding the theoretical convective heat transfer coefficient have been found in an article by D. Roncati [10]. To calculate a theoretical convective heat transfer coefficient, Grashof and Prandtl number must be calculated. Grashof number can be calculated using equation (2.11) and Prandtl by using equation (2.12).

$$Gr = \frac{g \cdot L^3 \cdot \beta \cdot (T_p - T_a)}{\eta^2} \tag{2.11}$$

g = Gravity (9,81 m/s^2)

L = Length of conductor (m)

β = Air thermal expansion coefficient 1/T_o (1/K)

T_s = Temperature of hot surface(K)

T_o = Temperature of air (K)

η = Air kinematic viscosity 1,807*10^-5 at 325 K (m^2/s)

$$\mathrm{Pr} = \frac{\mu \cdot c}{\lambda} \tag{2.12}$$

μ = Air dynamic viscosity at 325 K =1.962*10^-5 (kg/m*s)

c = Air specific heat 1006.3 at 325 K (J/(kg*K))

λ = Air thermal conductivity 0.02816 at 325 K (W/(m*K)

When Grashof and Prandtl number are found, Nusselt number can be calculated. Which equation used for calculating Nusselt number is determined by several factors. These can be type of convection, rotation of object, the air flow and the ratio between length and diameter. Equation (2.13) are chosen for the calculation of Nusselt number. The assumptions made by

choosing this equation is natural convection and laminar flow of the air inside the enclosure. The ratio between length and diameter are assumed to be small, and that the effects of curvature cannot be ignored. [11]

$$Nu = \frac{4}{3} \cdot \left(\frac{7 \cdot Gr \cdot Pr^2}{5 \cdot (20 + 21 \cdot Pr)} \right)^{\frac{1}{4}} + \frac{4(272 + 315 \cdot \mathrm{Pr}) \cdot L}{35 \cdot (64 + 63 \cdot Pr) \cdot D} \quad (2.13)$$

$Nu =$ Nusselt number

$L =$ Height of conductor (m)

$D =$ Diameter of conductor (m)

When Nusselt number have been found by using equation (2.13), the theoretical convective heat transfer coefficient can be calculated by using equation (2.14).

$$h_{conv} = \frac{Nu \cdot \lambda}{L} \quad (2.14)$$

$h_{conv} =$ Heat transfer coefficient (W/m^2*K)

$Nu =$ Nusselt number

$\lambda =$ Thermal conductivity (W/(m*K)

$L =$ Length of conductor (m)

2.4 Total heat transfer coefficient

When estimating the heat transfer there could sometimes be useful to find a common heat transfer coefficient. This coefficient includes the different effect of heat transfer. To find the total heat transfer coefficient equation (2.15) is used. This equation is the same as the second term in equation (2.5), in chapter 2.2 Heat Generation.[2]

$$P_{total} = h \cdot U \cdot (T_{conductor} - T_a) \quad (2.15)$$

P_{total} = Total power loss (W)

$h =$ Heat transfer coefficient (W/m^2*K)

$U =$ Surface area (m^2)

$T_s =$ Surface temperature (K)

$T_o =$ Ambient temperature (K)

Equation (2.15), shows that the ambient temperature shall be used to calculate the total heat transfer coefficient. The total heat transfer coefficient will include both convection and radiation. Since the convection is using the air temperature as ambient (equation (2.9)) and radiation is using the wall temperature as ambient (equation (2.8)), it will result in an error when calculating a total heat transfer coefficient. Which temperature (wall or air) to select as

ambient, depends on which of effect that is dominant. This means which of the effects (conduction or radiation) that are contributing to the highest power loss. [2]

3 Method

In this chapter, there will first be a description of the switchgears used during the experiments. Then the rest of the equipment needed to carry out these tests will be presented. In the last part of this chapter the different methods for performing the experiments is described.

3.1 System description

In this subchapter, information about the switchgears used in this report will be presented. The different test conducted in this report will be presented for both switchgears.

3.1.1 Switchgear with knife switch

In Figure 3-1, a picture of the 4-module switchgear is presented. The picture contains a name in each row (A0#) which will be used for referring to the different modules in the switchgears further in the report. This switchgear has knife switches in the 3 first modules (A01, A02 and A03). In the last module(A04) it is vacuum breakers installed.

Figure 3-1: Picture of the front of the 4-module switchgear.

When heating up the switchgear, A01 is used as inlet where the current injector is connected. The outlets of A03 is short circuit and A02 is disconnected. This is shown in Figure 3-2 where a sketch of the three first modules with knife switched are presented.

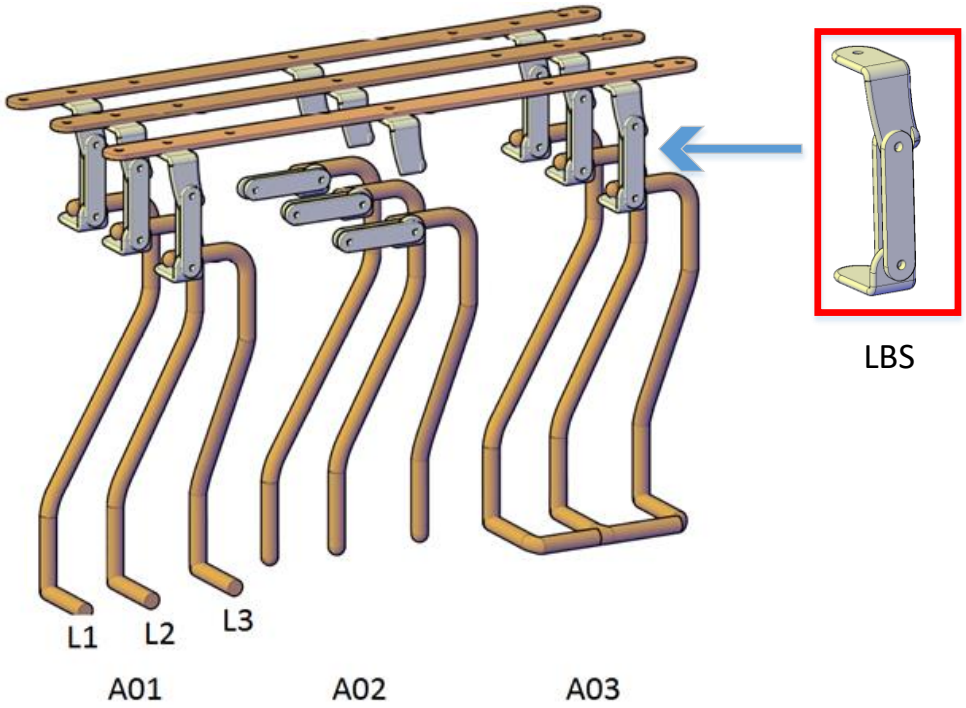

Figure 3-2: Illustration of the three first modules with knife switches.

The conductors in Figure 3-2 is placed inside an enclosure which normally is filled with SF_6 gas, but is instead filled with air during these tests. In Figure 3-2, a single knife switch is highlighted in the red rectangle. This illustration shows what is defined as the LBS for the knife switch design in this report. The contact resistance in the bolted connections between the busbar and the outlet rod is included in the resistance for the LBS.

For the switchgear with knife switches, two tests will be conducted in this report. Both tests will be conducted on the knife switch in position A01 L1. The first test will be a bare knife switch. The second test will be with the insulating lever surrounding the knife switch. These two cases are presented in Figure 3-3, where Test 1 (KB) is the bare switch and Test 2 (KE) is with the insulating lever.

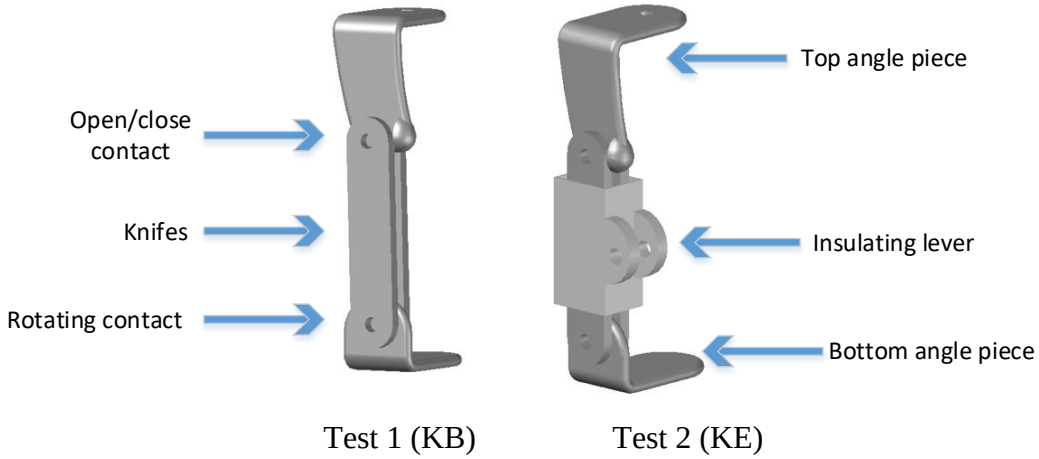

Figure 3-3: A representation of the two tests of the knife switch.

The dimensions of the knife switch are presented in Table 3-1. This table also contains the calculations of the surface area used further in this report.

Table 3-1: Dimensions of the knife switch and insulating lever.

Part	Width (mm)	Height (mm)	Depth (mm)	Surface (m^2)
Top angle piece	45	117	9	0,009346
Bare knife	24	113	12	0,007712
Bottom angle piece	40	75	9	0,00449
Insulating lever	30	45	35	0,00795
Visible of covered knife	24	68	12	0,004672

3.1.2 Switchgear with puffer switch

In Figure 3-4 , a picture of the 3-module switchgear with puffer switch is shown. The same naming of the module as explained in subchapter 3.1.1, will also be used in this subchapter. This switchgear has puffer switches in module A01 and A03. In A02 vacuum breakers are installed.

Figure 3-4: 3-module switchgear with puffer switch.

During the tests, A01 is used as an inlet and A03 is short circuited. A02 is disconnected allowing no current to run through the vacuum breakers. In Figure 3-5 a rough sketch of the conductors in the switchgear is shown.

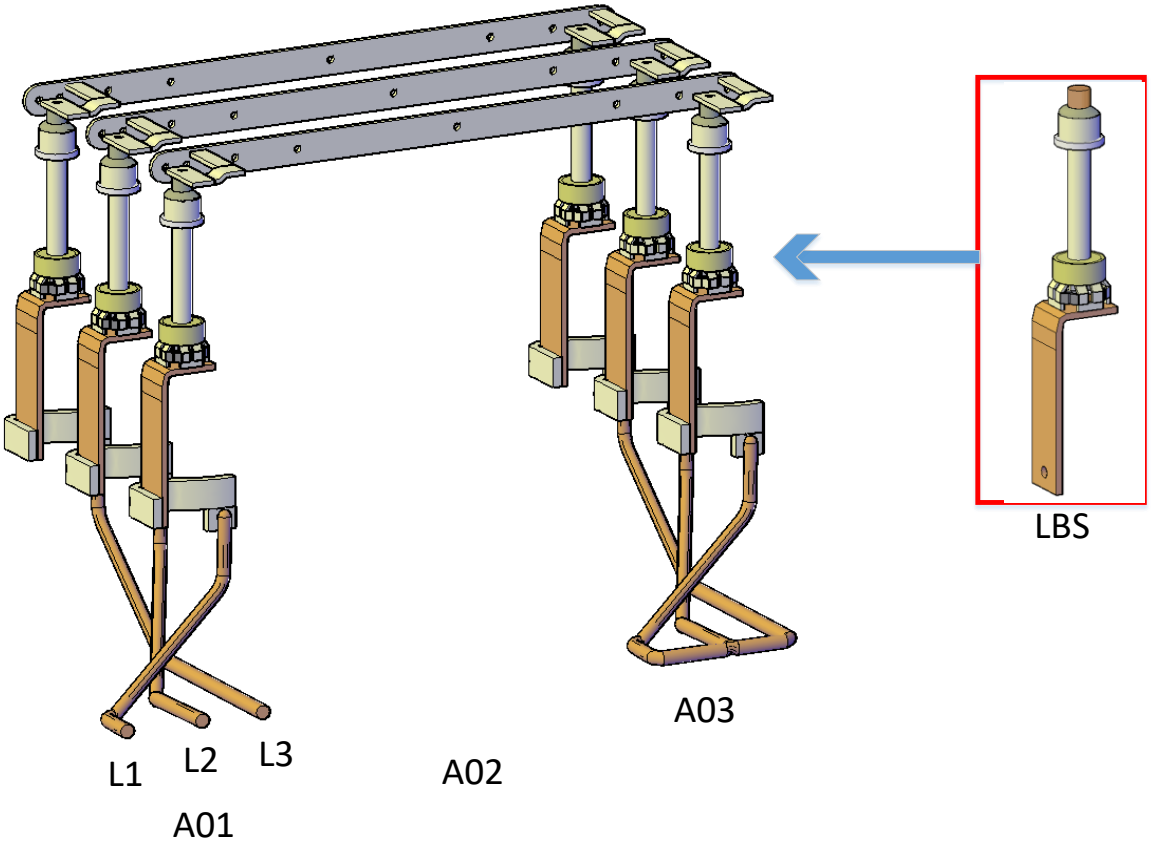

Figure 3-5: Illustration of the 3-module switchgear (without the vacuum breakers).

The conductors shown in Figure 3-5 is normally placed inside an enclosure filled with SF_6, but is instead filled with air during these tests. In Figure 3-5, A single puffer switch is shown in the red rectangle. This illustration shows what is defined as the LBS for the puffer switch design in this report. The contact resistance in the bolted connections between the puffer switch and the angle pieces in top and bottom is included in the resistance for the LBS. In this report, it is assumed that the influence of field controllers on the heat transfer from the LBS can be neglected. For all tests conducted, the field controllers have been removed from the puffer switch.

There will be performed three different test on the switchgear with puffer switches. The test object will be positioned in A03 L3. The first test will be a bare puffer switch. The second test will be a puffer switch with only the pressure cylinder. The last test will be a puffer switch with both pressure cylinder and crankcase. These three different types of setups are illustrated in Figure 3-6.

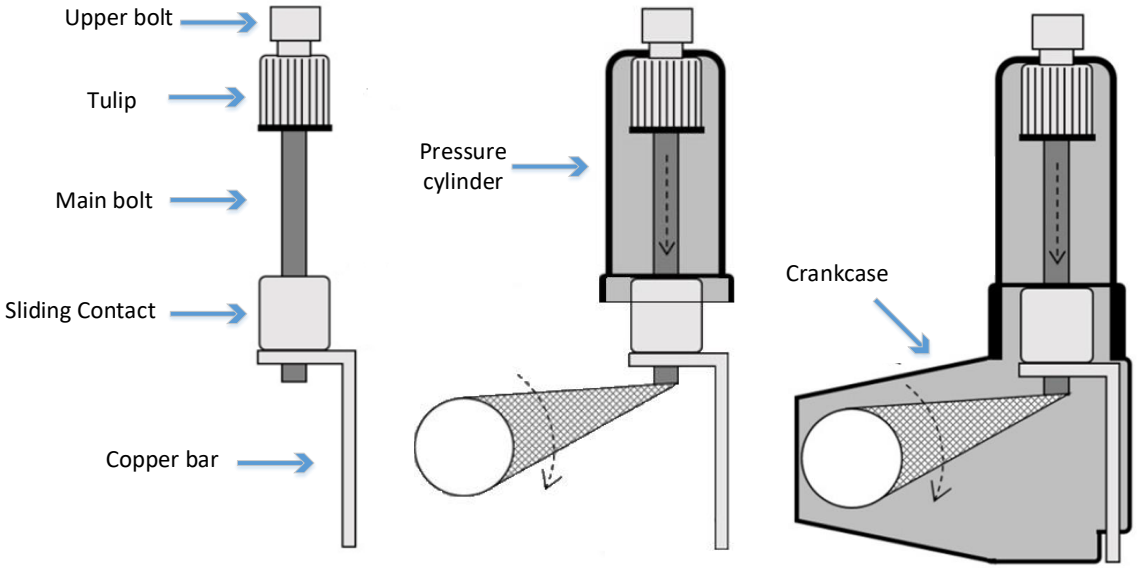

Test 3 (PB) Test 4 (PPC) Test 5 (PE)

Figure 3-6: A representation of the 3 test of the puffer switch. (figure 2 in [1])

In total, there will be five different tests on the two different switchgears. The five different tests are listed in Table 3-2. This table contains an explanation of the abbreviation used after the test numbers in this report.

Table 3-2: List of the different test conducted on the switchgears.

Test number	Abbreviation	LBS type	Type of encapsulation
1	KB (Knife bare)	Knife	Bare
2	KE (Knife encapsulated)	Knife	With insulating lever
3	PB (Puffer bare)	Puffer	Bare
4	PPC (Puffer pressure cylinder)	Puffer	With pressure cylinder
5	PE (Puffer encapsulated)	Puffer	With pressure cylinder and crankcase

The dimensions of the puffer switch are presented in Table 3-3. This table also contains the surface area for the different parts of the puffer switch, which will be used further in this report.

Table 3-3: Dimensions of the puffer switch and encapsulation.

Part	Width (mm)	Height (mm)	Depth (mm)	Radius (mm)	Surface (m^2)
Upper bolt		30		12,5	0,002356
Tulip		35		22	0,004838
Main bolt		115		7,5	0,005419
Sliding contact	20	30	20		0,0024
Cu-bar	40	130	7		0,01269
Pressure cylinder		160		80	0,0753
Crankcase	150	140	64		0,07912

3.2 Equipment used

The equipment used in this report to conduct the experiments is shown in Table 3-4.

Table 3-4: Table showing the equipment used in this report.

	Vendor	Type	Accuracy
Switchgear	ABB	4 modules	
Switchgear	ABB	3 modules	
IR-camera	Fluke	Ti25	± 2 ºC or 2 % (whichever is greatest)
Thermocouples		Type K	±0,004t or ±1,5°C
Current Injector	Hilkar	Ak23	
Multi meter	Gossen Metrawatt	High Resolution TRMS System Multimeter	Voltage DC – for 60 mV ± 30 µV

Clip-on current transformer	Gossen Metrawatt	Z3512	±(0.5% reading + 0.05A)
Logging device	Keysight	Agilent 34972A LXI Data Acquisition/ Switch Unit Software: BenchLink Data Logger 3	
Thermometer	Fluke	54 II B	

3.2.1 Thermocouple

For measuring the temperatures, thermocouples have been used. These sensors have two conductors that is in contact with each other in the measuring point. These conductors consist of two different types of semiconductors. This will create a small electric charge in the circuit, which will depend on the temperature where the two conductors meet. This voltage can be read, using a manual thermometer or a logging device. The thermocouples used during the experiments is type K class 1. Information about these thermocouples can be found in Table 3-5. [12]

Table 3-5: Thermocouple type K class 2 specifications [13].

Element type	Class	Standard range	Accuracy
K (Ni-Cr)	1	-40/1000 °C	± 0,004T or ± 1,5°

3.3 Finding the emissivity coefficient for a material

For finding the emissivity coefficient for the materials, an Infrared Camera was used. When using such a camera it is possible to measure either the temperature if the emissivity of the material is known, or the emissivity if the temperature is known. The switchgears were heated up with 630 A AC for an hour to get a temperature difference on the material from the ambient temperature. The temperature was measured with thermocouples of type K, presented in 3.2.1.

The emissivity coefficient on the IR-camera was changed until it measured the same temperature as the thermocouple. Some pictures were taken with the camera and the temperature readings of the thermocouples was written down. This method was repeated for the different materials.

When all the different materials had been measured, the pictures were analysed in FLUKE SmartView. This program gives the opportunity to find the maximal, minimal and average temperature in a region. It is also possible to change the emissivity after the picture is taken. [14]

3.4 Resistance measurement

This measurement was conducted by connecting a 100 A DC source to the system and measuring the voltage drop. The resistance was then calculated by the result of these measurements and compared with the values found in the previous tests.

The cold resistance was measured between each steady state test. This was done to confirm that the changes of the LBS did not affect the resistance. The warm resistance of the LSB designs were measured, by connecting the DC source instantaneously after the temperature measurements (explained in chapter 3.5). The total power loss of the switchgears was measured by using the two-wattmeter method.

3.5 Temperature measurements

When the switchgears were heated up to steady state the current injector was used. This was set to deliver 630 A AC at 50 Hz for all three phases. Then the temperatures were logged until the switchgears had reached steady state. The temperatures were read using thermocouples type K, presented in chapter 3.2.1. Thermocouples was placed inside the switchgears, both along the conductive parts, on the walls of the enclosure and in the air inside the enclosure. The room temperature was also measured. The room temperature was measured 1 meter away from the front of the switchgears. The placing of the sensors inside the switchgears were decided on what was needed, to be measured to find the desired result. A list of all the sensors and placing for the two different systems can be found in appendix B and appendix C. The next three subchapters will show where the sensors were placed and why these spots were selected.

3.5.1 For estimating the contribution of conduction

Conduction is the heat transfer from the LBS along the conductive path. Equation (2.7) ,in chapter 2.3.1 Conduction, shows what to measure for estimating the power loss due to conduction. The temperature difference between a known length need to be measured. This temperature difference was found by placing two thermocouples with a known distance along the conductor, both on the busbar and on the outlet rod. This make it possible to calculate the power loss to conduction for the LBS. The setup for measuring the conduction is shown in Figure 2-2.

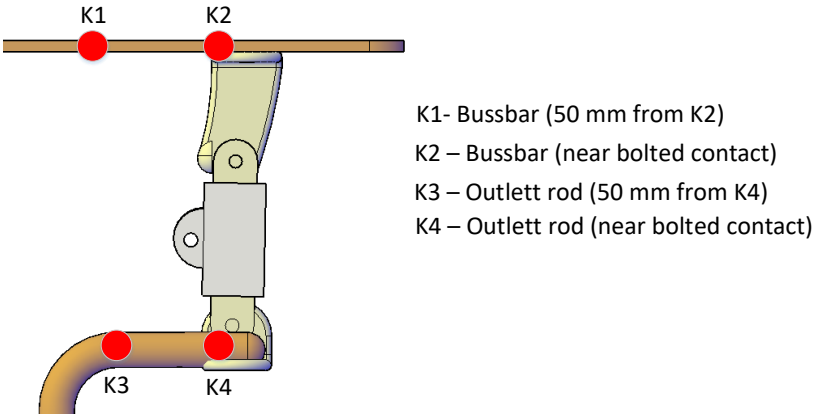

Figure 3-7: Setup for estimating conduction from the knife switch.

The conduction shall also be estimated for the puffer switch. For this LBS, it is desired to measure the conduction upward to the busbar and downwards to the outlet rod. The setup used for the puffer switch is shown in Figure 3-8.

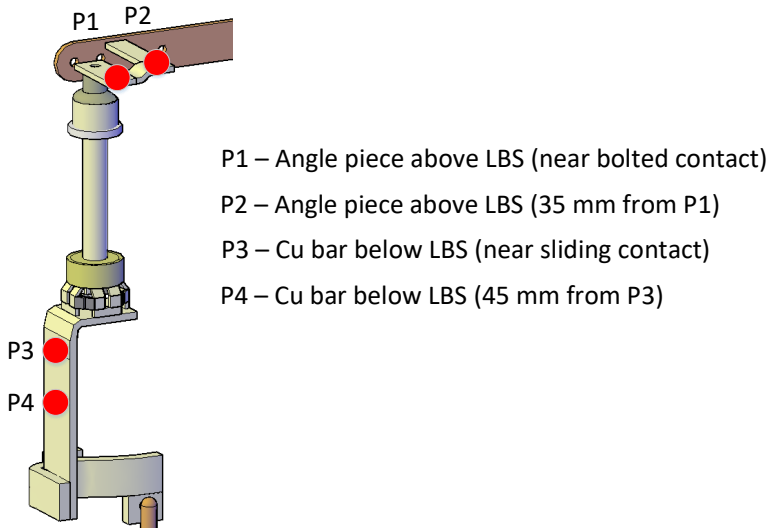

Figure 3-8: Setup for estimating conduction from the puffer switch.

When installing these sensors, the distance between them need to be decided. If the distance is long the effect of convection and radiation could influence the result. If they are placed too close together, there can be difficult to spot a difference in the readings. The uncertainty in the measurements of the distance also leads to uncertainty in the calculations. This uncertainty will be more dominant for shorter distances.

3.5.2 For estimating the contribution of convection

In equation (2.9), in chapter 2.3.3 Convection, the temperatures needed to calculate the convection is presented. These are the temperature of the air inside the switchgears and the temperatures of hot surfaces. To measure the temperature of the air surrounding the LBS inside the switchgear, a thermocouple was placed in the same height as the LBS. There were placed sensors on the different parts on both LBS, for measuring the temperatures of the hot surfaces. Figure 3-9 shows the points chosen to measure for calculation of the convection on the knife switch.

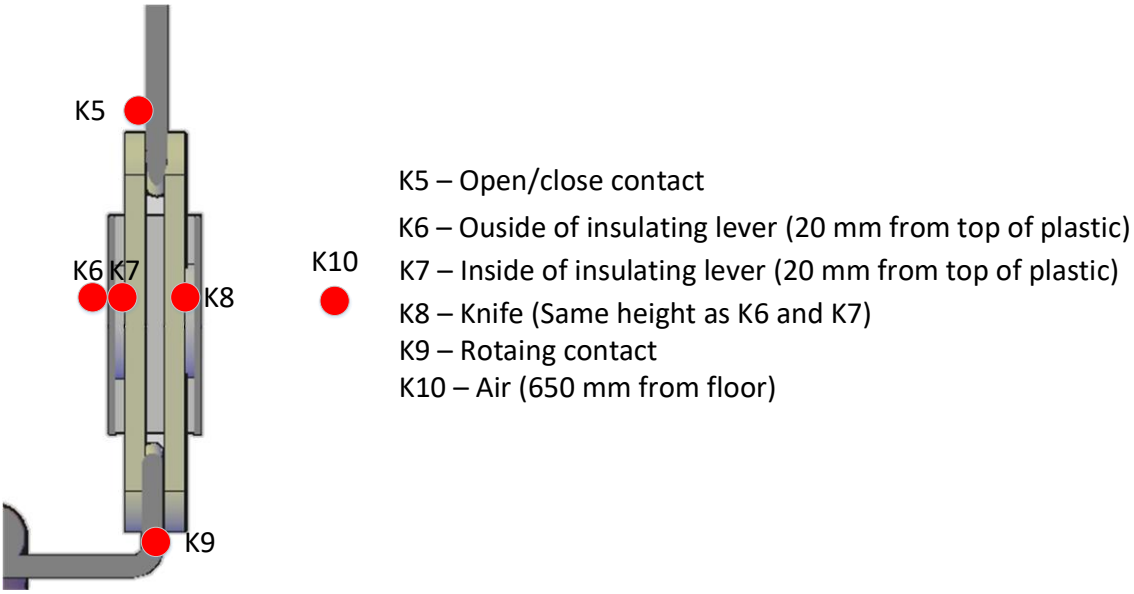

Figure 3-9: Setup for estimating convection on knife switch.

Figure 3-10 shows the points chosen for the bare puffer switch for estimating the convection.

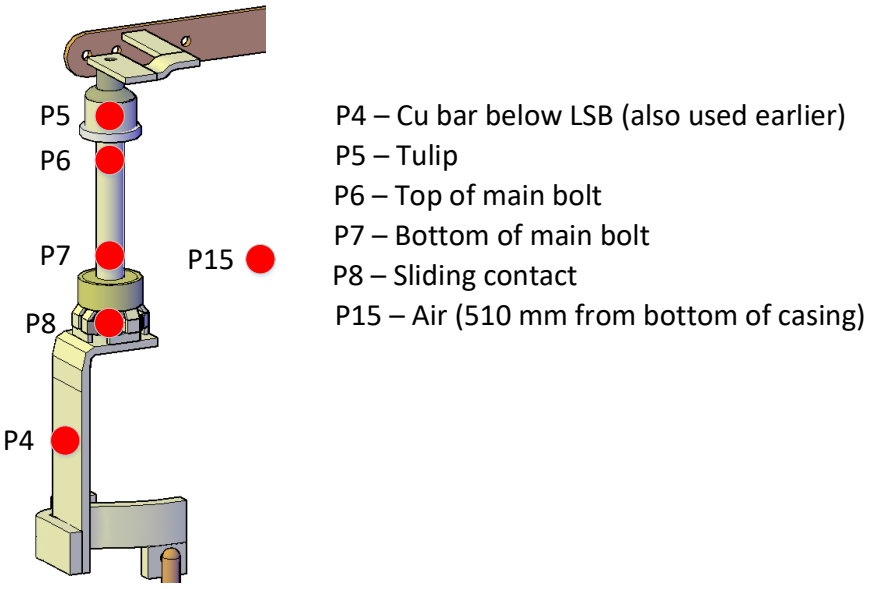

Figure 3-10: Setup for estimating convection on bare puffer switch.

Figure 3-11, shows the measuring points on the encapsulated puffer switch.

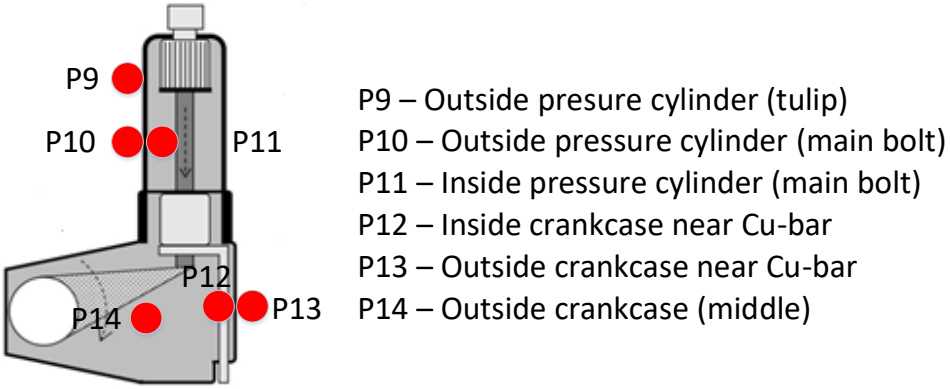

Figure 3-11: Setup for estimating convection on encapsulated puffer switch.

3.5.3 For estimating the contribution of radiation

Equation (2.8), in chapter 2.3.2 Radiation, shows that the temperatures needed to be measured is the temperature of the hot object and the wall temperature. The temperature of the hot object is already measured for the conduction shown in Figure 3-9 (for the knife switch) and Figure 3-10 and Figure 3-11 (for the puffer switch). The figures can be found in chapter 3.5.2. The wall temperature was measured by placing a thermocouple on the side wall of the enclosure, shown in Figure 3-12 for switchgear with knife switches. In Figure 3-13, the placement of the wall mounted thermocouple for the switchgear with puffer switches is shown. These were placed in the same height as the placement of the load break switch.

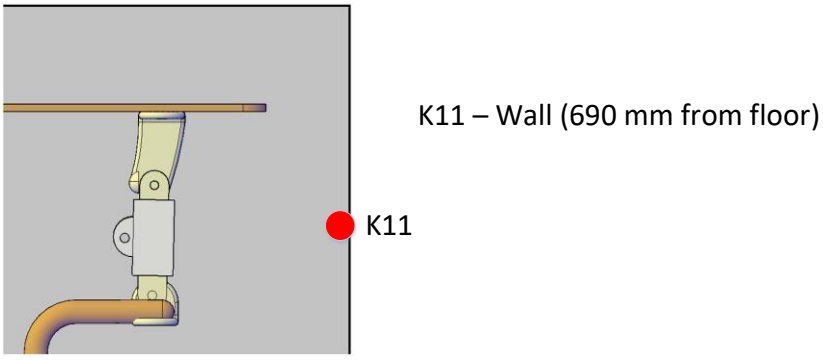

Figure 3-12: Placement of thermocouple mounted on the wall in switchgear with knife switches.

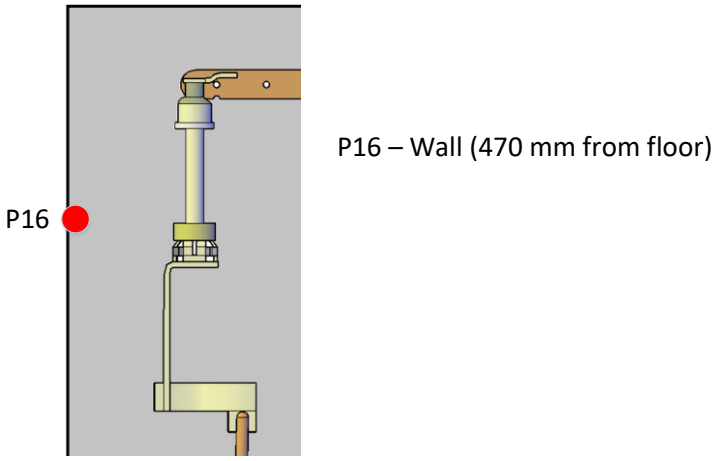

Figure 3-13: Placement of thermocouple mounted on the wall in switchgear with puffer switches.

4 Results

This chapter contains the results found in this report. First the power input in each test will be presented. Then the temperature measurements will be presented. In the last subchapter, the heat transfer calculation will be presented.

4.1 Power input

In this chapter the power input in the different tests will be presented. These will be used in the heat transfer calculations. In Table 4-1, the results of the power input are presented.

Table 4-1: Steady state resistance and power input.

Test number	Cold resistance (μΩ) in LBS	Steady state resistance (μΩ) in LBS	Power loss in LBS (W)	Total power loss in SWG (W)
Test 1 (KB)	35	44	17	350
Test 2 (KE)	34	44	17	343
Test 3 (PB)	54	60	24	340
Test 4 (PPC)	55	61	24	343
Test 5 (PE)	64	71*	28	340

*This resistance was not measured, but is instead calculated by looking at the percentage increase for the resistance of the previous tests, for the puffer switch.

Table 4-1 shows that the measured resistance in test 5 (PE) stands out in comparison with the previous tests. The resistance in test 5 (PE) has increased with 16 % from test 4 (PPC).

4.2 Temperature measurements

In this chapter, some of the temperature measurements will be presented. In appendix B, a complete list of the temperature measurements for the two tests of the knife switch can be found. For the three test on the puffer switch, the temperature measurements can be found in appendix C. All the temperatures presented in this chapter are temperature rise (ΔT) from ambient temperature. In Table 4-2 the measurements of the air and wall temperatures inside the enclosures are shown.

Table 4-2: Air and wall temperatures inside the enclosures

Test number	ΔT of air inside enclosure (ºC)	ΔT of wall inside enclosure (ºC)
Test 1 (KB)	30,5	15,1
Test 2 (KE)	31,2	16,2
Test 3 (PB)	31,1	19
Test 4 (PPC)	30,5	18,5
Test 5 (PE)	30,4	18,4

The results in Table 4-2, shows that the air temperatures and wall temperatures have not been changing for the tests conducted. This is as expected since the total power losses of the switchgears in Table 4-1, is stable.

In Figure 4-1 some of the measuring points along the knife switch are plotted. This gives an overview of the temperature changes of the conductive parts, in the two test, of the knife switch. In Figure 4-1, the point of congelation has been moved to 70 ºC, for a better visualization of the temperature trend.

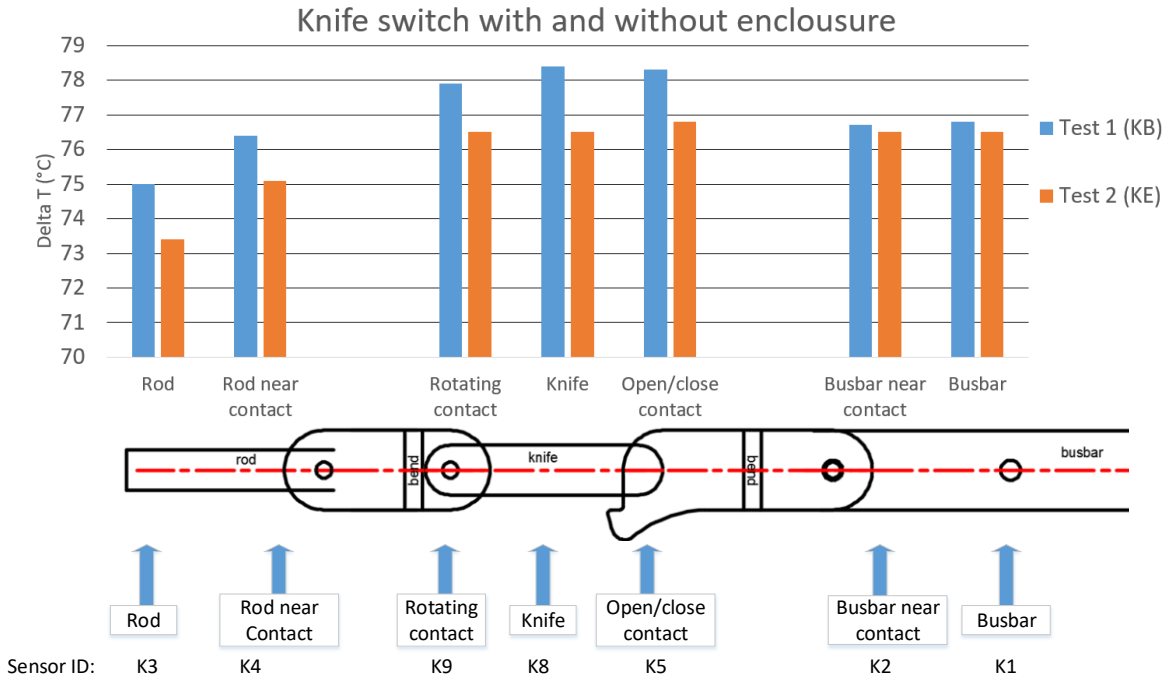

Figure 4-1: Temperature measurement on the knife switch with and without insulating lever.

Figure 4-1 shows a small increase in temperature when the insulating lever is removed. The temperature trend of both tests is comparable.

In Figure 4-2, a radially plot of the knife switch is presented. The plot shows the temperature from the conductor, out through the insulating lever, to the air inside the enclosure.

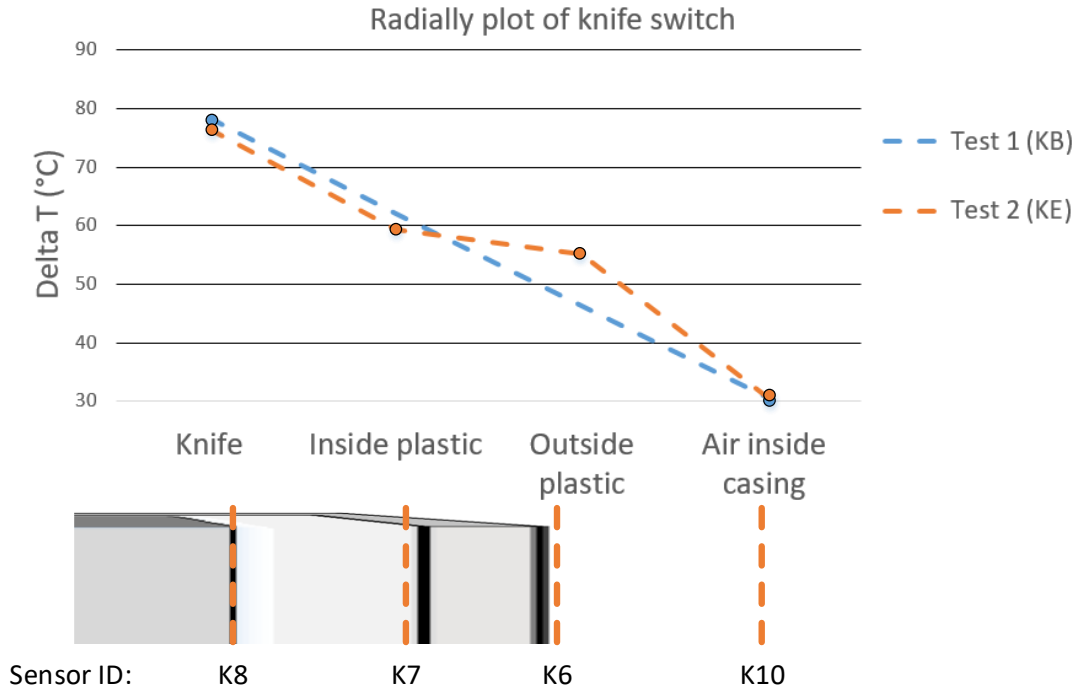

Figure 4-2: Radially plot of temperature differences in the knife switch throughout the insulating lever.

Figure 4-2 displays how the thermal conductivity is changing out through the encapsulation. The insulating lever has a higher thermal conductivity than air, which lead to less change in temperature through the lever than through the air. The dashed line between the measuring points in Figure 4-2 is only graphical representation of the temperature decrease and are not measured. These lines would be negative exponential lines and not linear as shown in the figure.

In Figure 4-3, some of the measuring points along the puffer switch are presented for all three tests. In the figure the point of congelation has been moved to 70 ºC, for a better visualization of the temperature trend.

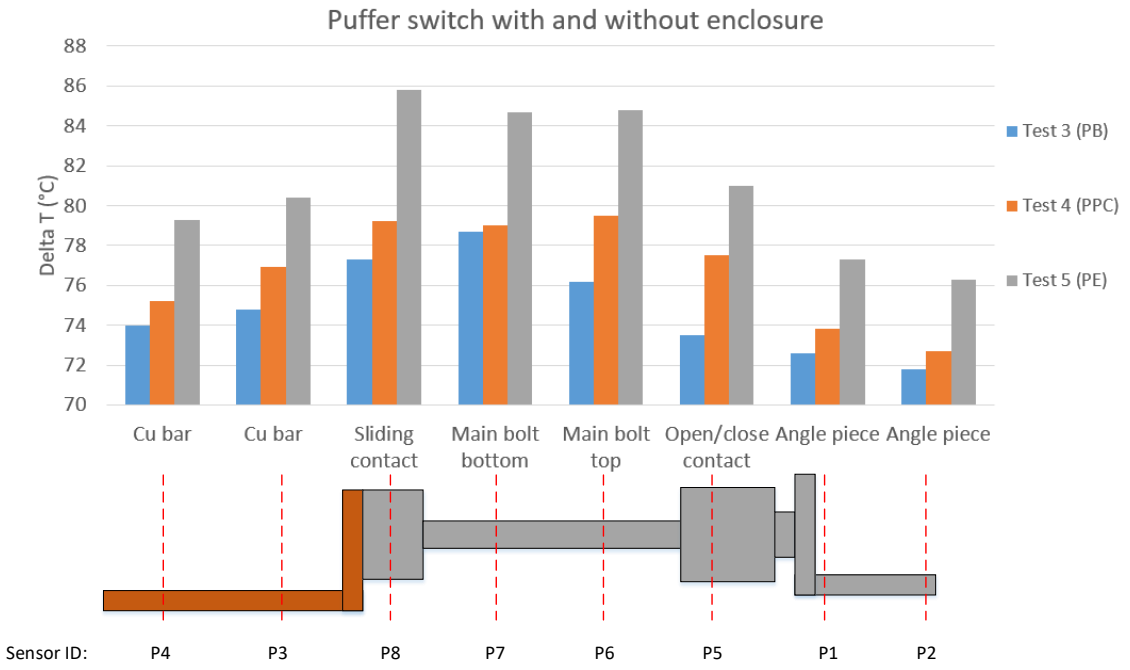

Figure 4-3: Displaying the temperature measurement of the puffer switch for the three tests.

The temperature results are presented as they are measured in Figure 4-3. There have been taken no consideration to the increase in resistance in test 5 (PE). Because of this an increase in the temperature measurements for test 5 (PE) in Figure 4-3 are expected. This will further be discussed in chapter 6.2.

There is also made a radially plot for the puffer switch. The plot shows the temperature from the conductor, out through the encapsulation, to the air inside the enclosure. This plot is shown in Figure 4-4.

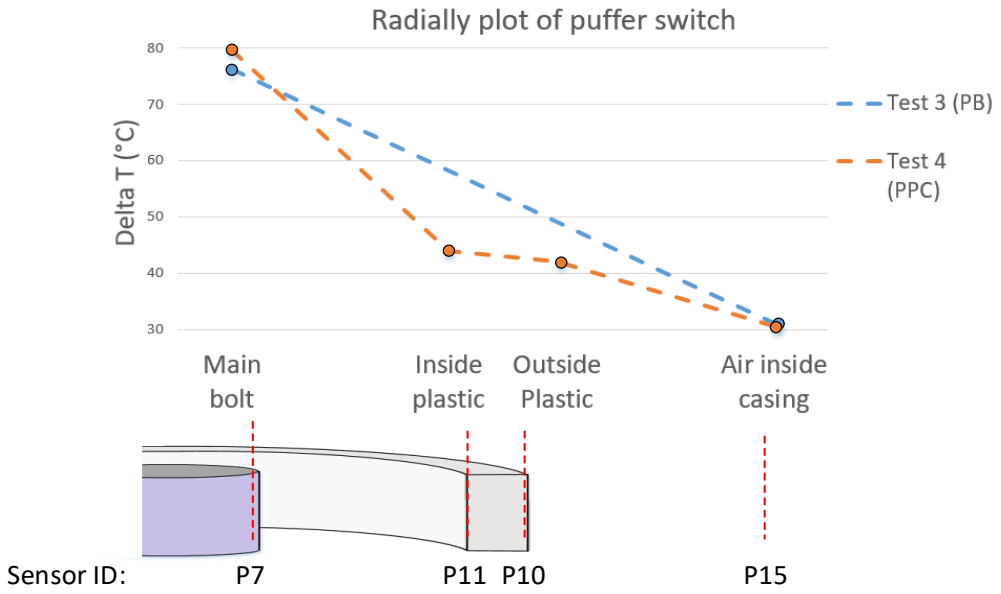

Figure 4-4: Radially plot the temperature difference on the puffer switch out through the encapsulation.

Figure 4-4 displays how the thermal conductivity is changing out through the encapsulation. The pressure cylinder has a higher thermal conductivity than air, which lead to less change in temperature through the cylinder than through the air. The dashed line between the measuring points in Figure 4-4 is only graphical representation of the temperature decrease and are not measured.

4.3 Heat transfer calculations

First in this chapter the emissivity coefficient measurements will be presented, which later are used in the calculations of radiation. The results from measurements of the emissivity coefficient is presented in Table 4-3. These values are an average for the different materials measured. Lexan 3413 was not measured, but instead found in literature[8].

Table 4-3: The emissivity coefficients used in the calculations.

Type of material	Emissivity coefficient	Measured
Copper	0,27	Yes
Lexan 3413[8]	0,89	No
PA-63 Trogamid T5000 NL	0,88	Yes
PBT- Tecodur PB70 NL IL	0,92	Yes
Silver coated copper	0,17	Yes

In Table 4-4, the distribution of how much each of the three heat transfer mechanisms is contributing in watt, for the different tests are presented. In these calculations, the conduction and radiation is calculated. Convection is found by assuming it will be the rest of the input power presented in Table 4-1. To calculate the surface area for each test, the dimensions presented in Table 3-1 (knife switch) and Table 3-3 (puffer switch) are used. The calculation for radiation and convection is calculated part by part as presented in Table 3-1 (knife switch) and Table 3-3 (puffer switch). The power loss of each part is added together to find the power loss for the different heat transfer mechanisms for each test. For more details of the calculations, see appendix D and appendix E

Table 4-4: Contribution of each heat transfer mechanism in LBS for the different tests.

Test number	Conduction (W)	Convection (W)	Radiation (W)
Test 1 (KB)	2,5	13,8	1,2
Test 2 (KE)	3,1	12,5	2,0
Test 3 (PB)	3,9	18,1	1,8
Test 4 (PPC)	6,9	8,1	9,2
Test 5 (PE)	4,7	9,8	13,7

Table 4-4 shows that the power loss due to conditions is not changing much, except the conduction for test 4 (PPC). This have increased by almost 47 % from the second highest power loss due to conduction for the puffer switch (Test 5). The calculations in appendix E, shows that it is the conduction downward to the outlet rod that have the highest increase in power loss. This will be discussed later in chapter 6.3 in Discussion. Table 4-4 shows that the power loss due to radiation have a huge increase for test 4 (PPC) and test 5(PE). This is affected by changes in the surface area and emissivity coefficient when encapsulating the conductor.

In Figure 4-5, the contribution of each heat transfer mechanism is presented in percentage. This gives a better understanding how the contribution of each effect is changing.

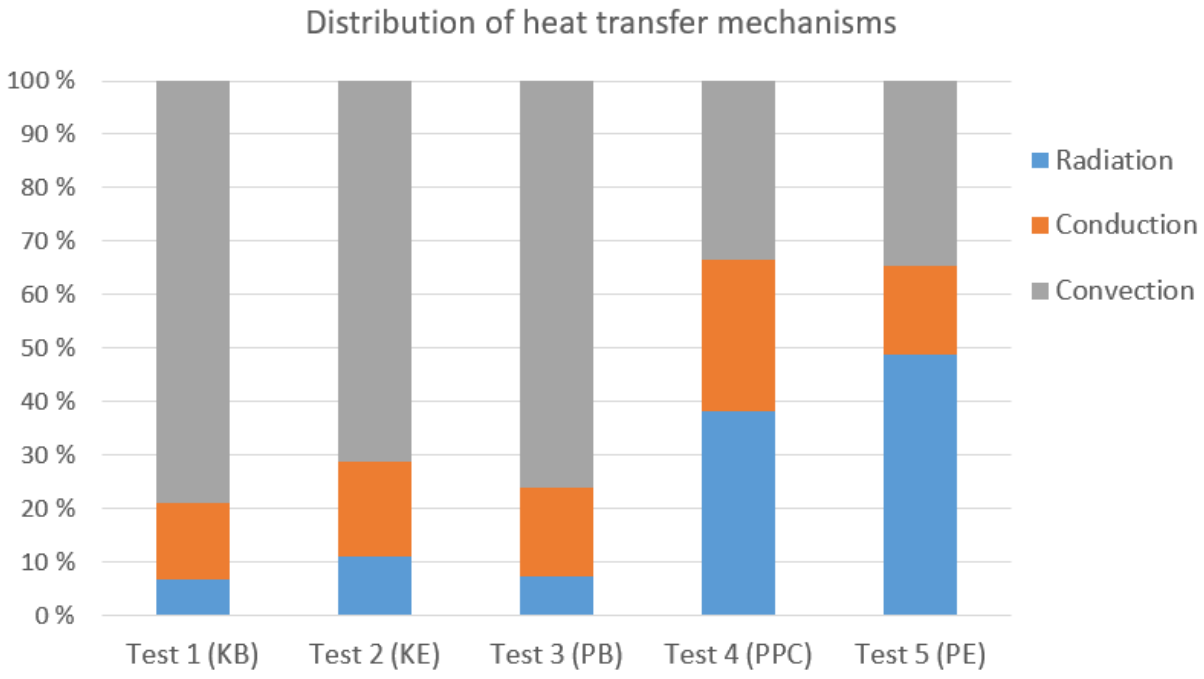

Figure 4-5: Distribution of heat transfer mechanisms for each test.

Figure 4-5 shows that the radiation is increasing in the tests with encapsulation. The reason why the encapsulation increases the power loss due to radiation are the change in emissivity, see Table 4-3, and the increasing surface area. The increase in the knife switch is not as big as for the puffer switch. This is due to the different extent of encapsulation of the two LBS designs.

In Table 4-5, the calculations of the empirical and the theoretical convective heat transfer coefficients are shown.

Table 4-5: Empirical versus theoretical convective heat transfer coefficient.

Test number	Empirical convective heat transfer coefficient (W/m^2*K)	Theoretical convective heat transfer coefficient (W/m^2*K)
Test 1 (KB)	13,4	5,6
Test 2 (KE)	12,1	5,0
Test 3 (PB)	15,1	5,4
Test 4 (PPC)	4,9	3,9
Test 5 (PE)	6,4	3,3

Table 4-5 shows that the theoretical calculations of the convective heat transfer coefficient are low when being compared with the empirical heat transfer coefficient. The theoretical values are following the same trend as the empirical values.

5 Theoretical calculations of encapsulation

In this chapter a theoretical approach to the heat transfer of an encapsulated cylinder will be examined. First an introduction to the effects of encapsulation and the model used for calculation is presented. Then the equations used for calculations will be introduced, before the results of the calculations is presented.

5.1 Introduction to encapsulation of conductors

When a conductor is encapsulated, it will affect the heat transfer from the conductor. When the radius of the encapsulation is increasing, it will create a bigger cooling surface. This will decrease the convection resistance. This will also affect the distance the heat must travel from the conductor to the surface, which will increase the conduction resistance. Because of these two effects, it is possible to find a critical radius. The critical radius is the radius where the conductor will have the greatest power loss. In some cases, adding encapsulation to a cylindrical conductor can increase the heat transfer from the conductor. This will depend of which of the effects, decreasing the convection resistance or increasing the conduction resistance, that are dominating. To calculate the critical radius equation (5.1) will be used.[15]

$$r_{critical} = \frac{\lambda}{h} \tag{5.1}$$

$r_{critical}$ = Critical radius (m)

λ = Thermal conductivity (W/m*K)

h = Heat transfer coefficient (W/ m^2*K)

When encapsulating a conductor, the emissivity will change. The conductors in both LBS have a low emissivity coefficient. Since the encapsulation material has a high emissivity coefficient, the power loss due to radiation will increase.

5.1.1 Thermal conductivity of air cavities

For the puffer switch, there are a considerable amount of air between the main bolt and the pressure cylinder. In this this subchapter, the effect of air cavities will be explained. Air at rest have a low thermal conductivity at 0.024, but in air cavities over a curtain size the air will no longer be at rest. This makes it complicated to look at air as a solid matter with a curtain thermal conductivity. The change in the thermal conductivity for air will be affected by radiation, conduction and if the cavity is ventilated. The area of the cavity will also affect the thermal conductivity, because in smaller cavities the air will be close to still. In bigger areas, the air flow will increase. There will not be conducted any calculations of the thermal conductivity for the air between the conductor and the encapsulation in this report, but an average thermal conductivity will be calculated in chapter 5.4.[16]

5.2 Simplified model of LBS

The knife switch is two parallel squared rods. There is a small air gap between the knifes and the encapsulation (2-4 mm). The puffer switch is a cylindrical rod, with a changing radius. The puffer switch has an air gap between the conductor and the isolation (67,5 mm). In Figure 5-1, an illustration of the encapsulated area for both LBS designs are presented.

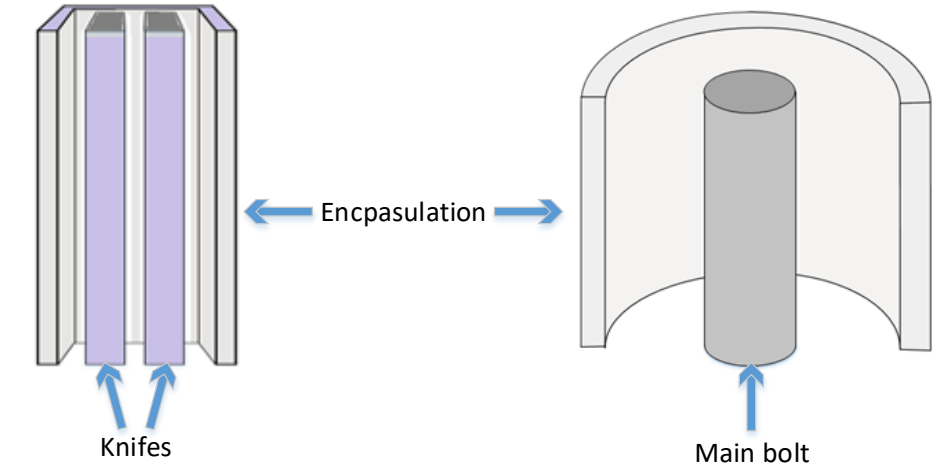

Knife switch Puffer switch

Figure 5-1: Illustration of the encapsulated area of both LBS designs.

For the theoretical calculations of heat transfer a simplified model have been made for both LBS designs. This model is containing a cylindrical conductor with a cylindrical encapsulation. There is no air gap between the conductor and the encapsulation. The model used for both LBS designs is shown in Figure 5-2.

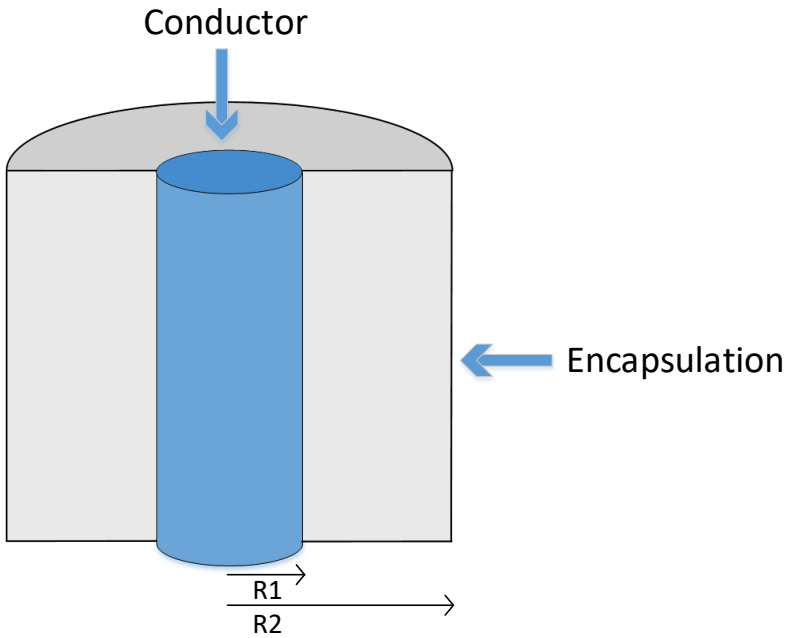

Figure 5-2: A simplified model of both LBS.

For both switches an average radius of the conductor must be found (R1 in Figure 5-2). An average radius should also be found for the encapsulation (R2 in Figure 5-2). This model of the LBS designs is assumed to be infinitely long, and will not have any power loss due to conduction.

5.3 Theory of encapsulation of a cylindrical conductor

For deriving an equation that can be used for a cylindrical conductor, Fourier's law of conduction is used. Fourier's law is shown in equation (5.2).

$$\dot{Q} = -\lambda \cdot U \cdot \frac{dT}{dr} \tag{5.2}$$

$\dot{Q} =$ Heat flow (W)

$\lambda =$ Thermal conductivity (W/m*K)

$U =$ Surface area (m^2)

$dT =$ Change in temperature (K)

$dr =$ Change in radius (m)

The equations for the heat transfer presented in chapter 2.3, Heat transfer, is derived from this equation. Since the model in this chapter is cylindrical, the equations will change because of the derivation of dr. From equation (5.2) an equation for calculating the conduction through a cylindrical object can be found, shown in equation (5.3). [15]

$$\dot{Q}_{conduction} = \frac{2 \cdot \pi \cdot L \cdot \lambda \cdot (T_s - T_0)}{\ln\left(\frac{r_2}{r_1}\right)} \tag{5.3}$$

$\dot{Q}_{conduction} =$ Heat flow (W)

$T_s =$ Temperature of conductor (K)

$T_0 =$ Temperature of the outer surface of encapsulation (K)

$r_1 =$ Radius of conductor (m)

$r_2 =$ Radius of encapsulation (m)

$L =$ Length of model (m)

$\lambda =$ Thermal conductivity (W/m*K)

The length of the model used in equation (5.3) is the length of the encapsulated area. For the knife switch this is defined as the height of the insulating lever. For the pressure cylinder the encapsulated area is defined as the length of the pressure cylinder.

5.4 Results of theoretical calculations of encapsulation

In this chapter equation (5.3) will be used to calculate an overall thermal conductivity constant throughout the encapsulation. For the calculations, the simplified model of the LBS will be used. This model is presented in chapter 5.2. When solving equation (5.3) for the thermal

conductivity, the heat flow becomes an input. To estimate a value for the power loss in the encapsulated area, an average power loss per length is found. In Table 5-1, the results of the thermal conductivity calculations are presented.

Table 5-1: Thermal conductivity constant calculations.

Type of switch	Power loss per length (W/m)	Length (m)	R1 (m)	R2 (m)	λ (W/m*K)
Knife	48	0.045	0,0115	0,0206	0,21
Puffer	51	0.16	0,0107	0,0825	0.45

These thermal conductivity constants together with the heat transfer coefficient, can be used in equation (5.1) to find the critical radius. The convective heat transfer coefficients are presented in Table 4-5 in chapter 4.3. In Table 5-2, the results of the critical radius calculations are presented.

Table 5-2: Critical radius calculations.

Type of switch	Critical radius (m)
Knife	0,0174
Puffer	0,0917

6 Discussion

In this chapter, the result presented in chapter 4 (Results) and chapter 5.4 (Results of theoretical calculations of encapsulation) will be discussed. First a short discussion of the emissivity measurement will be presented. Then the results of the knife switch will be discussed. In next section the discussion of the puffer switch is presented. Last in this chapter there will be a discussion of the theoretical convective heat transfer coefficient.

6.1 Emissivity measurement

When measuring the emissivity coefficient of materials with low emissivity, reflections of the surrounding temperatures could affect the result. This gives a bigger uncertainty in the measurements for the materials with low emissivity (copper and silver plated copper) [14]. In literature, the emissivity coefficient for matte copper is 0.22. For silver the emissivity coefficient is 0.01 and silver plated Nickel is 0.06.[17] .It is difficult to determine an uncertainty on the measurements presented (Table 4-3) in this report, but the values presented from the literature can give an indication. The uncertainties of the emissivity coefficients will affect the calculation of power loss due to radiation.

6.2 Knife switch

For the knife switch, there was no deviation in the steady state resistance and a small deviation in the cold resistance measurements. This deviation could be due to measuring error. If the deviation is caused by measuring error, it is more likely that the error has occurred when measuring the steady state resistance. When measuring the steady state resistance, the AC power supply must be disconnected to connect the DC power supply. When the 630 A AC is disconnected, the temperatures drops instantaneously. This will create a greater uncertainty in the measurement of the steady state resistance, compared to the cold resistance measurements.

In the temperature measurements for the knife switch, Figure 4-1 in chapter 4.2, it is a small difference in the measurements between the two tests. This support the theory that it could have been a measuring error in the steady state resistance, and that it could have been a higher resistance in test 1 (KB). The biggest difference in temperatures is in the area where the insulating lever was fitted in test 2 (KE). This may indicate that the insulating lever increases the heat transfer from the knife.

In the heat transfer calculations for the knife switch, there is a small deviation in power loss due to radiation between the two tests. This is caused by the change in emissivity when fitting the insulating lever. Even though the temperature of the hot surface (now being the lever) has decreased, the effect of the increasing emissivity and surface area is dominating. The reason why the power loss, due to radiation, do not have a bigger increase is because the insulating lever is covering only a small part of the knife switch. In test 2 (KE) there is a small increase in the conduction, which is strange since the temperature of the knife switch is lower than in test 1 (KB). This small increase is probably due to measuring error.

If the results for the theoretical average thermal conductivity (0,22 W/m*K) is compared with the thermal conductivity for the insulating lever (0,21 W/m*K [8]), the deviation between these values are small. The knife switch has a small air gap (2 - 4 mm) between the insulating lever

and the knife. The result of the average thermal conductivity shows that this air gap can be neglected when looking at the conductivity for the insulating lever.

If the result of the critical radius (0.0174 m) is compared with the approximation of the radius for the insulating lever (0.0203 m), the deviation is only 3,2 mm. This supports the temperature measurements that shows a small increase in the temperature when the insulating lever is removed. This effect of the insulating lever is so small it could be neglected, when estimating the temperature of the knife switch.

6.3 Puffer switch

For the puffer switch, there was only a small deviation at 1 μΩ for both cold and steady state resistance, for test 3 (PB) and 4 (PPC). For Test 5 (PE), the resistance has increased by 16 % from test 4 (PPC). Several attempts were made to reduce the resistance. The change in resistance was probably due to the fitting of the crankcase. The crankcase pulled on the main bolt, which lead to problems getting the main bolt in the same position as in the previous tests.

For the temperature measurements of the puffer switch (Figure 4-3) the difference in temperatures is as expected when comparing them to the increased resistance. If test 3 (PB) and test 4 (PPC) are compared, the greatest increase in temperatures are in the area where the pressure cylinder is fitted. The increased temperature in this area could indicate that the pressure cylinder decreases the heat transfer away from the puffer switch. Another reason, and perhaps more likely, is that the resistance in the open close contact has increased in test 4 (PPC). The temperature measurements for test 5 (PE) is difficult to compare with test 3 (PB) and 4 (PPC), because of the increased resistance. If an assumption is made that the temperature is linear with the power input, the temperatures would decrease with 14 %. If the open/close contact and the sliding contact is considered with these assumptions, the result in Table 6-1 is found.

Table 6-1: Reduction of temperatures in Test 5 (PE)

Measuring points	Temperatures from test 5 (PE) (ºC)	14 % reduction of temperatures in test 5 (PE) (ºC)	Temperatures from test 3 (PB) (ºC)
Open/close contact (P5)	81	70	73,5
Sliding contact (P8)	85,8	74	77

The results in Table 6-1 indicates, that if the resistance in Test 5 (PE) had been equal to the resistance in Test 3 (PB). The temperatures measurements for test 5 (PE), probably would be close to the measurements found in test 3 (PB)

Figure 4-3 shows that the hottest spot is in the sliding contact for test 5 (PE). This indicates that the resistance probably has increased in this area.

Looking at the results for the heat transfer calculations for the puffer switch (Table 4-4), it is a huge change in power loss due to radiation. The contribution of radiation is 7,4 % of the total

power loss in test 3 (PB) and 48,8 % for test 5 (PE). The increase in radiation is because of the changed emissivity coefficient and surface area. The change in emissivity will have a huge impact, because of the high percentage of encapsulation for the puffer switch. The surface area of test 3 (PB) compared with test 5 (PE) has increased by 495 %. Both the change in emissivity coefficient and surface area will contribute to a high increase in the effect of radiation, even though the temperature has decreased from the conductor to the encapsulation. The heat transfer calculations show that the effect of conduction increases in test 4 (PPC). The calculations of the conduction in Appendix E, shows that conduction downwards to the outlet rod has increased by 113%. From the temperature measurements in Figure 4-3, the temperature changes in test 4 (PPC) is in the upper part of the puffer switch. The reason why the conduction downwards has increase, could be due to changed cooling conditions in the sliding contact when the pressure cylinder is fitted. Another reason for the increase in conduction for test 4 (PPC) could be measuring error. The increase in power loss to conduction, affects the convective heat transfer coefficient, for test 4 (PPC) (Table 4-5 in chapter 4.3). If an assumption is made that the conductivity measurement is a measuring error and the power loss due to conduction for test 4 (PPC) is set equal to test 3 (PB), the result in Table 6-2 is found.

Table 6-2: Calculated convective heat transfer coefficient (with reduced conduction for test 4)

Test number	Empirical conductive heat transfer coefficient (W/m^2*K)
Test 3 (PB)	15,1
Test 4 (PPC)	6,7
Test 5 (PE)	6,4

Table 6-2, shows that with the assumption of an error in the measurements of conduction in test 4 (PPC), the convective heat transfer coefficient for this test would be in between test 3 and 5.

Looking at the results for the average thermal conductivity (0,45 W/m*K) and compare it with the thermal conductivity for the pressure cylinder (0,21 W/m*K)[18]. It shows that the thermal conductivity found in the calculations is almost twice as high as for the pressure cylinder. This could be explained by the theory presented in chapter 5.1.1, Thermal conductivity of air cavities. In the puffer switch, there is an air gap with radius of 0,0675 m. The air flow in this air gap will increase the thermal conductivity in the air, because of the contribution of convection and radiation. Since the conductor have a small emissivity coefficient (0,17), convection will have the highest contribution.

When looking at the critical radius calculations (0,0917 m), it seems a little high. The radius of the encapsulation is 0,0825 m. If the calculations are repeated with the convective heat transfer coefficient at 6,7 W/m^2*K, found in Table 6-2. The critical radius is found to be 0,0671 m. From the results found in the temperature measurements for the puffer switch, a critical radius close to 0.0671 m would be realistic.

6.4 Theoretical convective heat transfer coefficient

The calculations of the theoretical convective heat transfer coefficient, Table 4-5 in chapter 4.3, is low when being compared with the empirical convective heat transfer coefficient values. The reason why the theoretical calculations values are low could be due to the assumptions made for choosing the equation (2.13) ,for calculating Nusselt number. The air flow is assumed to be laminar, but could be turbulent due to the design of the conductors and LBS. If the flow of the air inside the enclosure is turbulent, the conductive heat transfer coefficient would increase[19]. The size of the vertical cylinder that equation (2.13) is fitted for is not mentioned, only that the relationship between the length and diameter is small. If equation (2.13) is meant for a bigger cylinder, the heat transfer could be less effective than for the size of conductors in the knife and puffer switch. [1]

7 Conclusion

The heat transfer mechanisms are affected by encapsulation of the LBS designs. The power loss due to radiation increases for both designs when the encapsulation is fitted. For the knife switch the contribution of radiation increased from 7 % to 11 % of the total power loss. For the puffer switch the contribution of radiation increased from approximately 7 % to 50 % of the total power loss. For the contribution of convection, a decrease was found when encapsulating the LBS designs. For the knife switch the decrease was from 80 % to 73 % of the total power loss and 76 % to 35 % for the puffer switch. The contribution of conductive heat transfer was stable approximately 15 % of the total power loss for both LBS designs.

The encapsulation of the knife switch does not increase the temperature of the knife. If the encapsulation affects the temperature of the knife switch at all, it would decrease the temperature. The critical radius (0,0174 m) is found to be equal to the approximated radius of the encapsulation (0,0206 m). This is an indication that the encapsulation could increase the heat transfer from the knife switch. The temperature measurements show that the decrease in temperature is small when the insulating lever is fitted. If the temperature of the knife switch shall be estimated, the insulating lever could be neglected.

This apply for the puffer switch as well, even though the critical radius (0,0671 m) is found to be a little lower than the radius of the conductor (0,825 m). The temperature measurement shows a small increase for encapsulated puffer switch in comparison with the bare puffer switch. These changes are small and the encapsulation could be neglected if an estimate of the temperatures of the puffer switch shall be found.

References

[1] W. R. E. Fjeld, S.T.Hagen, and M. Saxengaard, "Estimating the temperature rise of load break switch contacts in enclosed MV switchgear " presented at the CIRED, Glasgow, 2017.

[2] W. Rondeel, "Physics in Electrical Engineering Lectures , EP2416 , University College of Southeast Norway," Lectures, 03.02, 2017.

[3] ABB. (2017). *SF6-isolert ringkabelanlegg type SafeRing 12/24*. Available: http://www.abb.no/product/db0003db004279/c125739900636470c12572880049db09.aspx

[4] East Coast Power Systems. (2012, 11.05). *Different Types and Classifications of Switchgear Power Systems*. Available: http://www.ecpowersystems.com/resources/switchgear/different-types-and-classifications-of-switchgear-power-systems/

[5] Intergovernmental Panel on Climate Change. (2007, 11.05.17). *IPCC Fourth Assessment Report: Climate Change 2007*. Available: http://www.ipcc.ch/publications_and_data/ar4/wg1/en/ch2s2-10-2.html

[6] *IEC 62271-1: 2011 ed. 1.1, High voltage switchgear and controlgear - Part 1: Common specifications*, 2011.

[7] ABB. (2015). *Breakthroughs in switchgear technology with eco-efficient gases as an alternative to SF6*. Available: http://engineering.electrical-equipment.org/others/gas-insulated-vs-air-insulated-substations.html

[8] Saudi Basic Industries Corporation. (2017). *LEXSAN Resin 3413R*. Available: https://www.sabic-ip.com/gepapp/eng/weather/weatherhtml?sltRegionList=1002002001&sltPrd=1002003051&sltGrd=1002012239&sltUnit=0&sltModule=DATASHEETS&sltVersion=Internet&sltType=Online

[9] W. R. E. Fjeld, K. Vaagsaether, M. Saxengaard, P. Skryten and E. Attar, "Thermal design of future medium voltage switchgear," presented at the CIRED, Lyon, 2015. Available: http://cired.net/publications/cired2015/papers/CIRED2015_1090_final.pdf

[10] D. Roncati, "Iterative calculation of the heat transfer coefficient," Available: http://lisafea.com/pdf/Convection_heat_transfer_coefficient.pdf

[11] Y. Jaluria, "Natural Convection," New Brunswick, New Jersey: Rutgers University, 2002, pp. 545-546. [Online]. Available: https://s3-ap-southeast-1.amazonaws.com/erbuc/files/5165_cd5734dd-0bfc-444c-bf4c-7bfa2dccf870.pdf.

[12] J. Sandsten. (2009, 07.05.17). *Termoelement*. Available: https://snl.no/termoelement

[13] AUTEK. *Temperatur*. Available: http://autek.no/wp-content/uploads/temperaturkatalog.pdf

[14] L. T. Clausing, "Emissivity: Understanding the difference between apparent and actual infrared temperatures," p. 6Accessed on: 07.05Available: http://support.fluke.com/find-sales/Download/Asset/2563251_6251_ENG_B_W.PDF?trck=emissivityexplanation

[15] P. Talukdar. (2012, 03.08). *1D Steady state heat conduction (2)*. Available: http://web.iitd.ac.in/~prabal/MEL242/(6-7)-1-D-SS-Conduction-part2.pdf

[16] Metal Cladding and Roofing Manufactures Association, "Conventions for calculating U-values, F-values and Psi-values for metal cladding systems using two- and three-dimensional thermal calculations," pp. 13-15Available: http://www.mcrma.co.uk/pdf/mcrma_t18.pdf

[17] Omega. (2005). *Table of Total Emissivity*. Available: http://www.omega.com/temperature/Z/pdf/z088-089.pdf

[18] Plastiques Hautes Technologies. (2012). - *TROGAMID T 5000* -. Available: https://www.pht-plastic.com/app/download/8590571421/FICHE_PA6_T5000-gb.pdf?t=1383588383

[19] HRS Heat Exchangers. (17.08). *Comparison of Laminar and Turbelent Flow*. Available: https://www.hrs-heatexchangers.com/resource/comparison-laminar-turbulent-flow/

Appendices

Appendix A: Task description

University College of Southeast Norway

Faculty of Technology, Natural Sciences and Maritime Sciences, Campus Porsgrunn

FMH606 Master's Thesis

Title: Application of heat transfer coefficients for temperature rise calculations of MV switchgear

HSN supervisor: Elin Fjeld and Wilhelm Rondeel (co-supervisor)

External partner: ABB AS, EPMV

Task background:
Medium voltage (MV) switchgears are applied in the distribution network to ensure a safe and reliable power supply to the customers. The electrical equipment in the switchgear will experience a rise in temperature during normal operation due to ohmic losses. If the temperature rise is too high, the switching device may be degraded and ultimately not be able to perform its task. Especially critical are the different kind of electrical contacts. To avoid premature degradation of the equipment, any new switchgear design must undergo thermal testing to make sure the temperature rises are within the allowable industry limits set by the International Electrotechnical Commission (IEC).

SF_6 gas has been used for several decades to ensure the reliability and compactness of the switchgears. Unfortunately, SF_6 suffers from a very high global warming potential, and it is desirable to replace this gas in the future with more environmentally friendly gases, for example air. However, the poor thermal properties of air requires better thermal designs in order to keep the temperature rise within the allowable limits.

ABBs division in Skien are working to prepare the scientific and technological basis for future generation air filled MV switchgears. The University College of Southeast-Norway (HSN) is engaged in this research project together with ABB, and are dealing with the thermal design. The goal is to develop a design tool that can be used to predict the temperature rise of critical parts in future designs. The temperature rise of the air inside a sealed MV switchgear can be estimated with good precision by using the empirical method proposed by the IEC TR 60890. The next step is to determine the over-temperature of the current path (relative to the air inside the switchgear) by applying heat transfer coefficients.

One of the challenges is that the conductors and contacts of the LBS may be fully or partly (depending on the LBS design) enclosed by structures that are necessary for the switch to function properly. These structures will affect the heat exchange since the radiation and convection from the heat source (current path) is restricted, while the total surface area for heat exchange with the surrounding air is increased.

Task description:
The proposed Master's thesis will be a part of the ongoing research project between HSN and ABB. The student should calculate heat transfer coefficients for critical parts by considering the different heat transport mechanisms (convection, radiation, conduction). Temperature measurements should be performed with and without including the structures and the student should investigate how these structures affect the heat transport away from the hot spots.

Student category:
IIA students, preferably a student participating in the SCE4006 Project group SIV_08_16 "Power loss and temperature rise in a four-module switchgear".

Practical arrangements:
Two switchgear installations (provided by ABB) are available at HSN, a 3-module switchgear equipped with a puffer-type LBS and a 4-module switchgear equipped with a knife blade switch. A current injection system is also available which can supply continuous currents up to 2500 A AC (50 Hz) and 100 A DC.

Signatures:

Student (date and signature): Stein Gjygarden 27/1-17

Supervisor (date and signature): 27/1-17 Elisabeth Tidd

Address: Kjølnes ring 56, NO-3918 Porsgrunn, Norway. **Phone:** 35 57 50 00. **Fax:** 35 55 75 47.

Appendix B: Temperature measurements of knife switch

4-module SWG with Knife switches

Temperatures at stable conditions						Test 1 (KB) 630 A		Test 2 (KE) 630 A	
						T_abs	ΔT	T_abs	ΔT
Sensor pos.		Label	Sensor ID	Relevant info:		[°C]	[°C]	[°C]	[°C]
1	Ambient	A17				20,8		21,1	
Conductors:									
2	Open/close contact	A11	K5			99,1	78,3	97,9	76,8
3	Knife near plastic	A04	K8			99.2	78,4	89,5	76,5
4	Rotating contact	A10	K9			98,7	77,9	97,6	76,5
5	Busbar near contact	A13	K2			97,5	76,7	97,6	76,5
7	Busbar	A02	K1	50	mm from pkt. 5	97,6	76,8	97,6	76,5
8	Cu-rod below LBS	A08	K4			97,2	76,4	96,2	75,1
10	Cu-rod below LBS	A07	K3	70	mm from pkt. 8	95,8	75	94,5	73,4
Air inside SWG:									
12	Air temp	C04	K10	690	mm from floor	51,3	30,5	52,3	31,2
Enclosure walls:									
14	Venstre yttervegg	A05	K11	650	mm from floor	35,9	15,1	37,3	16,2
Natural enclsure:									
15	Ouside of insulating lever	C01	K6	20	mm insulating lever from top			76,2	55,1
16	Innside of insulating lever	C11	K7	20	mm insulating lever from top			80,4	59,3

Appendix C: Temperature measurements of puffer switch

3-module SWG with puffer switches

Temperatures at stable conditions						Test 3 (PB)	
						630 A	
						T_abs	ΔT
Sensor pos.		Label	Sensor ID	Relevant info:		[°C]	[°C]
1	Ambient	A17				21,5	
Conductors:							
2	Main bolt bottom	b20	P7			100,2	78,7
4	Angle piece above LBS	c14	P1			94,1	72,6
5	Angle piece above LBS	b01	P2	35	mm from pkt 4.	93,3	71,8
6	Tulip	c12	P5			95	73,5
7	Cu-bar below LBS	c08	P3			96,3	74,8
8	Cu-bar below LBS	c05	P4	45	mm from pkt 7.	95,5	74
9	Slideing contact	b19	P8			98,8	77,3
10	Main bolt top	b18	P6			97,7	76,2
Air inside SWG:							
11	Air temp	c07	P15	510	mm from floor	52,6	31,1
Enclosure walls:							
13	Right wall	c16	P16	470	mm from floor	40,5	19
Natural enclosure:							
18	Outside pressure cylinder (tulip)		P9				
19	Outside pressure cylinder (main bolt)		P10				
20	Inside pressure cylinder (main bolt)		P11				
22	Outside crankcase (middle)		P14				
24	Inside crankcase near Cu-bar		P12				
25	Outside crankcase near Cu-bar		P13				

3-module SWG with puffer switches

Temperatures at stable conditions						Test 4 (PPC)		Test 5(PE)	
						630 A		630 A	
						T_abs	ΔT	T_abs	ΔT
Sensor pos.		Sensor ID	Relevant info:		Label	[°C]	[°C]	[°C]	[°C]
1	Ambient				A17	23,1		23,8	
Conductors:									
2	Main bolt bottom	P7			c12	102,1	79	108,5	84,7
4	Angle piece above LBS	P1			c14	96,9	54,2	101,1	77,3
5	Angle piece above LBS	P2	35	mm from pkt 4.	b01	95,8	53,2	100,1	76,3
6	Tulip	P5			c15	100,6	57,9	104,8	81
7	Cu-bar below LBS	P3			c08	100	57,3	104,2	80,4
8	Cu-bar below LBS	P4	45	mm from pkt 7.	c05	98,3	56,2	103,1	79,3
9	Slideing contact	P8			b19	102,3	62,7	109,6	85,8
10	Main bolt top	P6			b18	102,6	61,7	108,6	84,8
Air inside SWG:									
11	Air temp	P15	510	mm from floor	c07	53,6	7,3	54,2	30,4
Enclosure walls:									
13	Right wall	P16	470	mm from floor	c16	41,6	-4,7	42,2	18,4
Natural enclsure:									
18	Outside pressure cylinder (tulip)	P9			a18	72,1	26	72,9	49,1
19	Outside pressure cylinder (main bolt)	P10			c06	66,2	18,5	65,4	41,6
20	Inside pressure cylinder (main bolt)	P11			b20	67	19,5	66,4	42,6
22	Outside crankcase (middle)	P14			c13			62,2	38,4
24	Inside crankcase near Cu-bar	P12			c04			71,2	47,4
25	Outside crankcase near Cu-bar	P13			c11			68	44,2

Appendix D: Calculation of power loss for the heat transfer mechanisms for the knife switch

Power loss due to radiation

Emissivity coefficients	
silvercoated copper	0,17
Insulating lever	0,89

$$P_{radiation} = \varepsilon \cdot \sigma_s \cdot U \cdot (T_s^4 - T_0^4) \cdot f$$

Constants used in equation	
Boltzmann	5,67E-08
Kelvin	273,15
Constant for surroundings	0,8

	Test 1 (KB)		Test 2 (KE)	
Parts	Surface (m^2)	ΔT	Surface (m^2)	ΔT
Top angle piece	0,009346	78,3	0,009346	76,8
Knife	0,007712	78,4	0,004672	76,5
Insulating lever			0,00795	55,1
bottom angle piece	0,00449	77,9	0,00449	76,5

Power loss to radiation	Test 1 (KB)	Test 2 (KE)
Top angle piece	0,504391	0,47380576
Knife	0,41723929	0,23500179
Insulating lever		1,02263076
Bottom angle piece	0,23991854	0,22584718
Total	1,16154883	1,9572855

Power loss due to conduction

Thermal conductivity for copper (W/m K)	400

$$P_{conduction} = \frac{\lambda}{L} \cdot A \cdot \Delta T$$

Downwards towards the outlet rod	Test 1 (KB)	Test 2 (KE)
Length (m)	0,07	0,07
Temp diff. (°C)	1,4	1,7
Cross-sec (m^2)	0,000314159	0,00031416
Power loss due to conduction (W)	2,513274123	3,05183286

Upwards towards the busbar	Test 1 (KB)	Test 2 (KE)
Length (m)	0,05	0,05
Temp diff. (°C)	-0,1	0
Cross-sec (m^2)	0,00024	0,00024
Power loss due to conduction (W)	-3,36E-05	0

	Test 1 (KB)	Test 2 (KE)
Total power loss due to conduction (W)	2,513240523	3,05183286

Power loss due to convection

Kelvin (K)	273,15

	Test 1 (KB)			Test 2 (KE)		
Parts	Surface (m^2)	% of total surface	ΔT	Surface (m^2)	% of total surface	ΔT
Top angle piece	0,009346	0,433729348	78,3	0,009346	0,353239096	76,8
Knife	0,007712	0,357898645	78,4	0,004672	0,176581752	76,5
Insulating lever	0	0	0	0,00795	0,300476226	55,1
bottom angle piece	0,00449	0,208372007	77,9	0,00449	0,169702925	76,5

Total	0,021548	Average temp of LBS (°C)	78,2524411	0,026458	Average temp of LBS (°C)	70,1757805

Case	Test 1 (KB)	Test 2 (KE)
Total areal (m^2)	0,021548	0,026458
Temp LBS (K)	351,402441	343,3257805
Temp air (K)	303,65	304,35
P_total (W)	17,4636	17,4636
h_tot	17,0	16,9
P_rad (W)	1,16	1,96
% radiation	6,7	11,2
P_cond (W)	2,51324052	3,051832863
% conduction	14,4	17,5
P_conv (W)	13,8	12,5
% convection	79,0	71,3
h_conv	13,4	12,1

Appendix E: Calculation of power loss for the heat transfer mechanisms for the puffer switch

Power loss due to radiation

Emissivity coefficients	
silvercoated copper	0,17
Copper	0,27
Presure Cylinder	0,88
Crankcase	0,92

$$P_{radiation} = \varepsilon \cdot \sigma_s \cdot U \cdot (T_s^4 - T_0^4) \cdot f$$

Constants used in equation	
Boltzmann	5,67E-08
Kelvin	273,15
Constant for surroundings	0,7

	Test 3 (PB)		Test 4 (PPC)		Test 5 (PE)	
Parts	Surface (m^2)	ΔT	Surface (m^2)	ΔT	Surface (m^2)	ΔT
Tulip	0,00719425	73,5	0,01994911	49,00	0,01994911	49,10
main bolt	0,00541925	77,45	0,06283185	42,10	0,06283185	41,60
Sliding contact	0,0024	77,3				
copper rod	0,01222	74	0,01222	75,2	0,07912	36,2

Power loss to radiation	Test 3 (PB)	Test 4 (PPC)	Test 5 (PE)
Tulip	0,41	2,46	2,48
main bolt	0,28610566	5,80	5,68
bot	0,12628799	0,00	0,00
rod	0,94790637	0,98085421	5,5838371
Total	1,77	9,24	13,75

Power loss due to conduction

Thermal conductivity for copper (W/m K)	400

$$P_{conduction} = \frac{\lambda}{L} \cdot A \cdot \Delta T$$

Downward towards the outlet rod	Test 3 (PB)	Test 4 (PPC)	Test 5 (PE)
length (m)	0,045	0,045	0,045
temp diff. (°C)	0,8	1,7	1,1
cross-sec (m^2)	0,00028	0,00028	0,00028
Power loss due to conduction	1,99111111	4,23111111	2,73777778

upward towards the busbar	Test 3 (PB)	Test 4 (PPC)	Test 5 (PE)
length (m)	0,035	0,035	0,035
temp diff. (°C)	0,8	1,1	0,8
cross-sec (m^2)	0,00021	0,00021	0,00021
Power loss due to conduction	1,92	2,64	1,92

	Test 3 (PB)	Test 4 (PPC)	Test 5 (PE)
Total power loss due to conduction	3,91111111	6,87111111	4,65777778

Power loss due to convection

Kelvin (K)	273,15

Test 3 (PB)

Parts	Surface (m^2)	% of total surface	ΔT
Tulip	0,007194247	0,26416908	73,5
Main bolt	0,005419247	0,198991992	77,45
Sliding contact	0,0024	0,088126773	77,3
Copper rod	0,01222	0,448712155	74
Total	0,027233495	Average temp of Conductor (°C)	74,84525619

Test 4 (PPC)

Parts	Surface (m^2)	% of total surface	ΔT

Tulip	0,019949113	0,209988531	49
Main bolt	0,062831853	0,661381199	42,1
Sliding contact			
Copper rod	0,01222	0,12863027	75,2
Total	0,095000966	Average temp of Conductor (°C)	47,80658281

Test 5 (PE)

Parts	Surface (m^2)	% of total surface	ΔT
Tulip	0,019949113	0,123218	49,1
Main bolt	0,062831853	0,38808819	41,6
Sliding contact			
Copper rod	0,07912	0,488693809	36,2
Total	0,161900966	Average temp of Conductor (°C)	39,88518843

$$P_{conv} = P_{total} - P_{cond} - P_{rad} \qquad P_{total} = h \cdot U \cdot (T_{conductor} - T_a)$$

	Test 3 (PB)	Test 4 (PPC)	Test 5 (PE)
Total areal	0,02723349	0,09500097	0,16190097
Temp Conductor (K)	348,325	320,9565828	313,0351884
Temp air (K)	304,25	303,65	303,55
P_total (W)	23,814	24,2109	28,1799
h_total	19,8	14,7	18,4
P_radiation (W)	1,77	9,2	13,7
% radiation	7,4	38,2	48,8
P_conducion (W)	3,9	6,9	4,7
% conduction	16,4	28,4	16,5
P_convection (W)	18,1	8,1	9,8
% conv	76,1	33,4	34,7
h_conv	15,1	4,9	6,4